INL/EXT-19-53792

Systems Research Supporting Standards and Interoperability (GM0085) Final Report

Don Scoffield (INL)
Zonggen Yi (INL)
Anudeep Medam (INL)
Jason Harper (ANL)
Myungsoo Jun (NREL)
Rick Pratt (PNNL)
Jonathan Coignard (LBNL)

April 2019

The INL is a U.S. Department of Energy National Laboratory operated by Battelle Energy Alliance

Idaho National Laboratory

INL/EXT-19-53792

Systems Research Supporting Standards and Interoperability (GM0085) Final Report

Don Scoffield (INL)
Zonggen Yi (INL)
Anudeep Medam (INL)
Jason Harper (ANL)
Myungsoo Jun (NREL)
Rick Pratt (PNNL)
Jonathan Coignard (LBNL)

April 2019

Idaho National Laboratory
Idaho Falls, Idaho 83415

http://www.inl.gov

Prepared for the
U.S. Department of Energy
Vehicle Technologies Office
Under DOE Idaho Operations Office
Contract DE-AC07-05ID14517

ABSTRACT

The objective of this project is to research the technical challenges and solutions on the integration of plug-in electric vehicles (PEV) into the grid. This project conducted the research by leveraging capabilities of multiple national laboratories with vehicle/grid integration (VGI) to perform hardware-in-the-loop (HIL) studies that integrate communication and control system with simulation and analysis activities. The PEV charging coordination research in this project has been performed on two main application cases at both residential locations and commercial buildings.

A highly efficient centralized residential PEV charging strategy has been developed for large PEV populations. This strategy designed a hierarchical optimization routine that aggregates individual PEV charging flexibility to reduce the computational complexity of the optimization process. The charging control strategy has been validated on the developed residential PEV charging research platform, which is based on high-fidelity, validated charging system models and charging behavior models. The developed charging control framework has been demonstrated to be capable of effectively coordinating the charging of 500,000 PEVS in about 5 seconds using a standard desktop computer. The impacts of developed charging strategy on residential distribution feeder, e.g. voltage support and capacity deferral, have been studied under different PEV penetration scenarios.

This project also studied PEV charging at commercial locations by building and operating a multi-laboratory platform for development and testing of aggregator-assisted control. This PEV charging strategy has been designed to include the local building level control and global aggregator level's optimal coordination for peak reduction. The impact on the distribution feeder of PEV charging controlled by commercial buildings has been investigated using the developed testing platform by studying three scenarios: uncontrolled, local building controlled and aggregator-assisted controlled. The analyses on the control strategy performance and overall system design structure helped to identify the unsolved technical challenges and to introduce potential solutions which can balance the competing objectives and interests between buildings and the distribution feeder.

CONTENTS

FIGURES

TABLES

ACRONYMS

ALAP	as late as possible
ANL	Argonne National Laboratory
ASAP	as soon as possible
BEMS	building energy management system
DRTS	digital real-time simulator
EV	electric vehicle
INL	Idaho National Laboratory
IoT	Internet of Things
LAN	local area network
MQTT	Message Queuing Telemetry Transport
NREL	National Renewable Energy Laboratory
PEV	plug-in electric vehicle
PG&E	Pacific Gas & Electric
PNNL	Pacific Northwest National Laboratory
SOC	state of charge
UI	user interface
WAN	wide area network

GM0085 Project Final Report

1. INTRODUCTION

As plug-in electric vehicles (PEVs) increasingly penetrate the marketplace, the integration of electric vehicles into the grid is essential to ensure the continued reliability and security of the grid. It has been widely proposed that PEVs can provide valuable grid services, such as load shifting to provide energy storage capacity for wind and solar generation, frequency regulation, and volt/volt-ampere reactive (VAR) support. However, significant technical challenges remain before this vision becomes reality. Prior to broad investment in the technical and business processes required for PEVs to provide grid services, fundamental questions must be answered, such as the following:

- How can PEVs provide grid services to effectively realize anticipated benefits to the grid without negatively impacting the grid or PEV owners?
- What communications requirements need to be put in place to facilitate PEVs providing grid services?
- What measurement and control challenges must be addressed to optimally utilize PEVs as a grid resource?

This project has researched the relevant technical challenges and solutions to facilitate the integration of electric vehicles into the grid. Five laboratories have participated in this project: INL, ANL, NREL, PNNL, and LBNL. The PEV charging research in this project has been conducted from multiple scenarios at both residential locations and commercial buildings.

First, this project has developed a hardware-in-the-loop platform to study integration of numerous electric vehicles on a residential distribution feeder. Using this platform uncontrolled and controlled electric vehicle charging has been analyzed for many different electric vehicle penetration scenarios. A key deliverable of this project is a PEV charging control strategy that effectively flattens the residential load profile while ensuring electric vehicle owners charging needs are met. This control strategy has been implemented by using an aggregator model that acts as an intermediary between the utility and residential distribution feeder. This work is further explained in Chapter 2.

Second, this hardware-in-the-loop platform was used to study the integration of PEV charging at commercial buildings. This phase of research aimed to understand the grid services potential of multiple commercial buildings coordinating their PEV charging via a centralized aggregator. The aggregator model communicated and coordinated the PEV charging at buildings located at ANL, PNNL, and NREL. This work is further explained in Chapter 3.

2. RESEARCH OF PEV CHARGING AT RESIDENTIAL LOCATIONS

The initial focus of this project was to understand the grid impacts of uncontrolled Level 2 charging of plug-in electric vehicles (PEVs) at residential locations. Key insights from The Electric Vehicle (EV) Project were used to understand the charging behavior of PEV owners and the implications of that behavior for PEV charge load management. These insights from the EV Project concluded that:

1. Most PEV charging occurred at home. For example, individuals who drove Nissan LEAFs charged at home 84% of the time when workplace charging was not available, and 65% of the time when workplace charging was available [1].
2. Uncontrolled residential PEV charging in the evening hours was coincident with the peak of the non-PEV residential load. This increased the peak and the rate of ramping present in the residential load, both of which are undesirable from the perspective of the electric utility [2].

3. Individuals tended to connect their PEVs to chargers shortly after the last trip of the day but did not disconnect their PEVs until the next morning, just prior to the first trip of the day. As a result, PEVs typically were connected to chargers all night with the opportunity to charge that entire time [3].

It became obvious during the EV Project that residential PEV charging could be made much more grid-friendly by shifting the PEV charging energy from peak-load hours to early morning hours when the non-PEV load is at its minimum (see Figure 1).

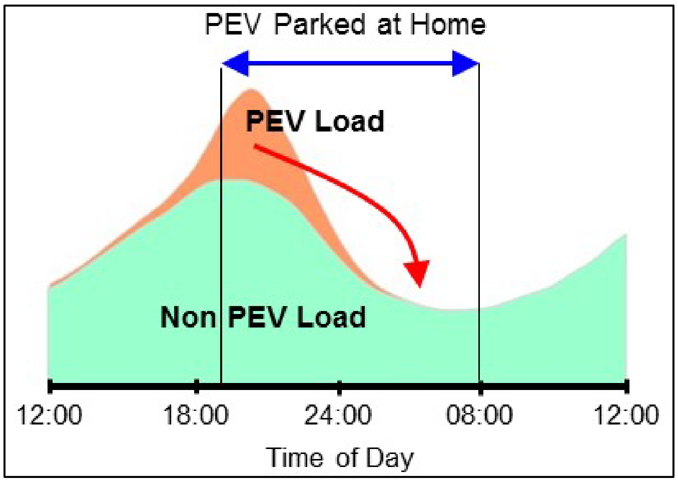

Figure 1. Uncontrolled residential PEV charging is coincident with non-PEV residential load because individuals tend to connect their PEVs to chargers after the last trip of the day and an uncontrolled PEV charger begins charging immediately after a PEV is connected. PEV charging could be made grid-friendly by shifting the PEV charging to early morning hours.

2.1 Residential PEV Charging Research Platform

As part of the GM0085 Project, a platform was created to study the grid impacts of PEV charging at residential locations (see Figure 2). This platform enables the following activities:

- Research of the grid impacts of uncontrolled PEV charging
- Development of PEV charging control strategies
- Investigation of the benefit of the PEV charging control strategies

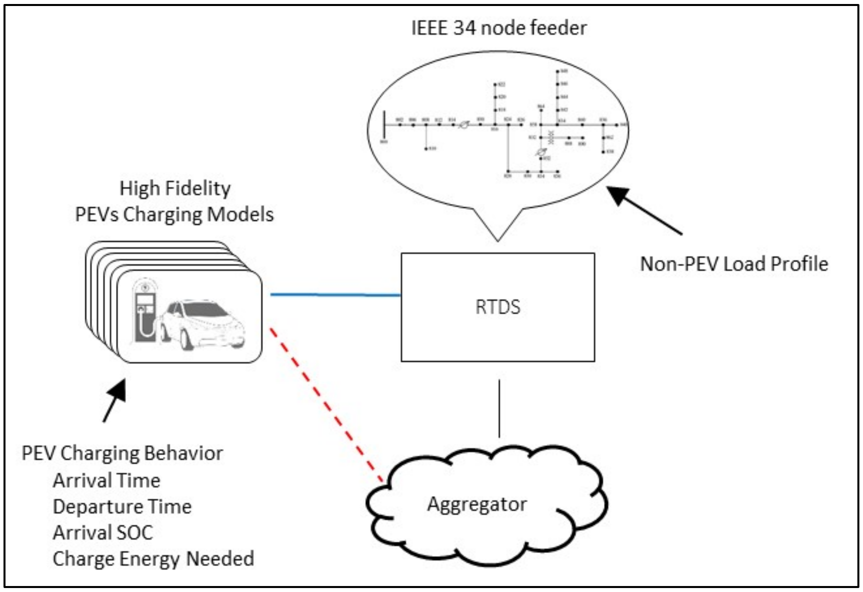

Figure 2. Platform to research the grid impacts of uncontrolled PEV charging, develop PEV charging control strategies, and investigate the benefit of the PEV charging control strategies.

This research platform contains the following important components:

- High-fidelity PEV charging models
- Grid Impacts Simulation Environment (RTDS, IEEE 34 node test feeder, Non-PEV Load Profile)
- Residential PEV charging Aggregator

The high-fidelity PEV charging models and grid impacts simulation environment are described in Sections 2.1.1 and 2.1.2, respectively. The residential PEV charging aggregator is described in Section 2.2.

2.1.1 High-fidelity PEV Charging Models

To understand how PEV charging affects the electric grid, it is essential to accurately model two aspects of PEV charging, PEV charging behavior and how PEVs behave as loads on the grid.

To model PEV charging behavior, PEV charging behavior data is used to initialize the high-fidelity PEV charging models. PEV charging behavior describes where and at what time PEV owners choose to charge their PEVs. PEV charging behavior data consists of the following:

- Time PEV connected to charger
- Time PEV disconnected from charger
- Battery state of charge (SOC) when PEV started charging
- Requested charge energy
- PEV charge location

PEV charging behavior data used in the research platform is derived from actual charging behavior data in The EV Project from the Pacific Gas & Electric (PG&E) service territory for 2013 Nissan LEAFs. The methodology used to derive PEV charging behavior data from the historical charging data is described in Ref. [4].

To model how PEVs behave as loads on the grid, high-fidelity charging models were created for the 2015 Nissan LEAF from laboratory testing results. These laboratory testing results were used to both create and then validate the PEV charging models.

Figure 3 and Figure 4 show a comparison of the output of the PEV charging model with the laboratory testing results for the 2015 Nissan LEAF. Figure 3 shows that the charging model output is a high-fidelity representation of:

- Efficiency as a function of charge rate
- Power factor as a function of charge rate
- Maximum charge rate as a function of battery SOC
- Power and current limits as a function of voltage

Figure 4 demonstrates that the representation of the transitions from one charge rate to another charge rate of the charging model for a 2015 Nissan LEAF is sufficiently accurate for understanding the impacts of PEV charging on the grid and developing PEV charging controls.

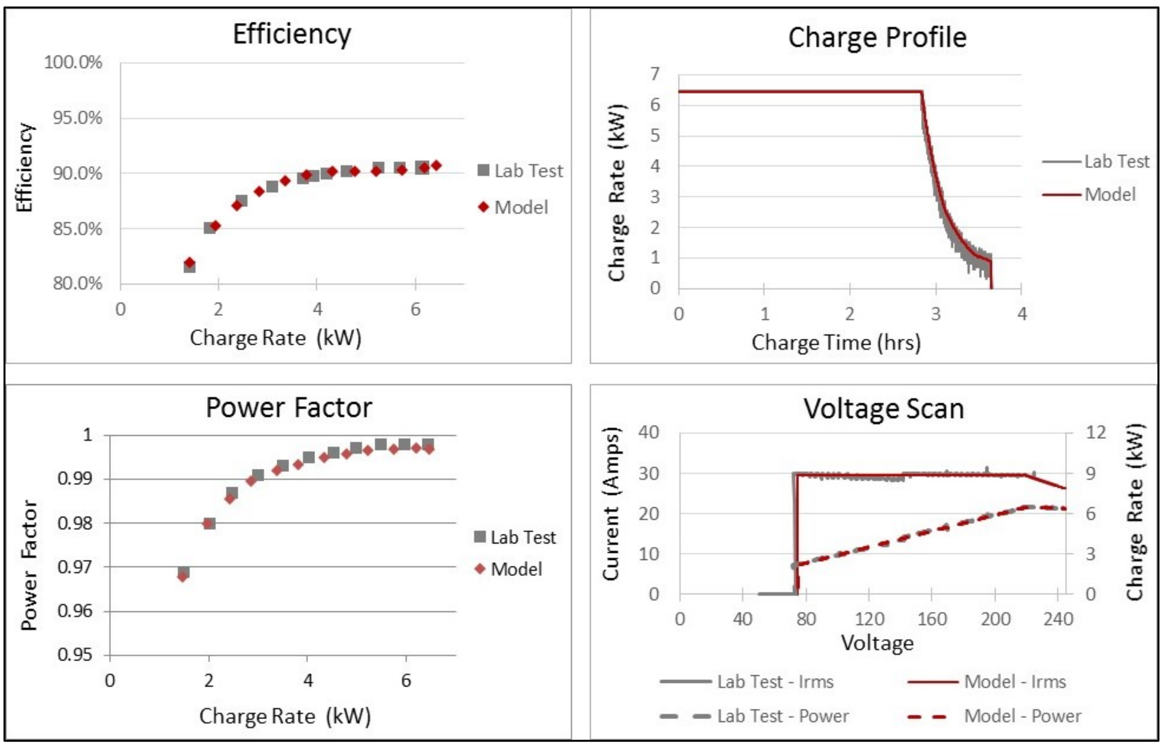

Figure 3. Comparison of laboratory test and model output results for a 2015 Nissan LEAF. The model output accurately represents the charging behavior of the 2015 Nissan LEAF.

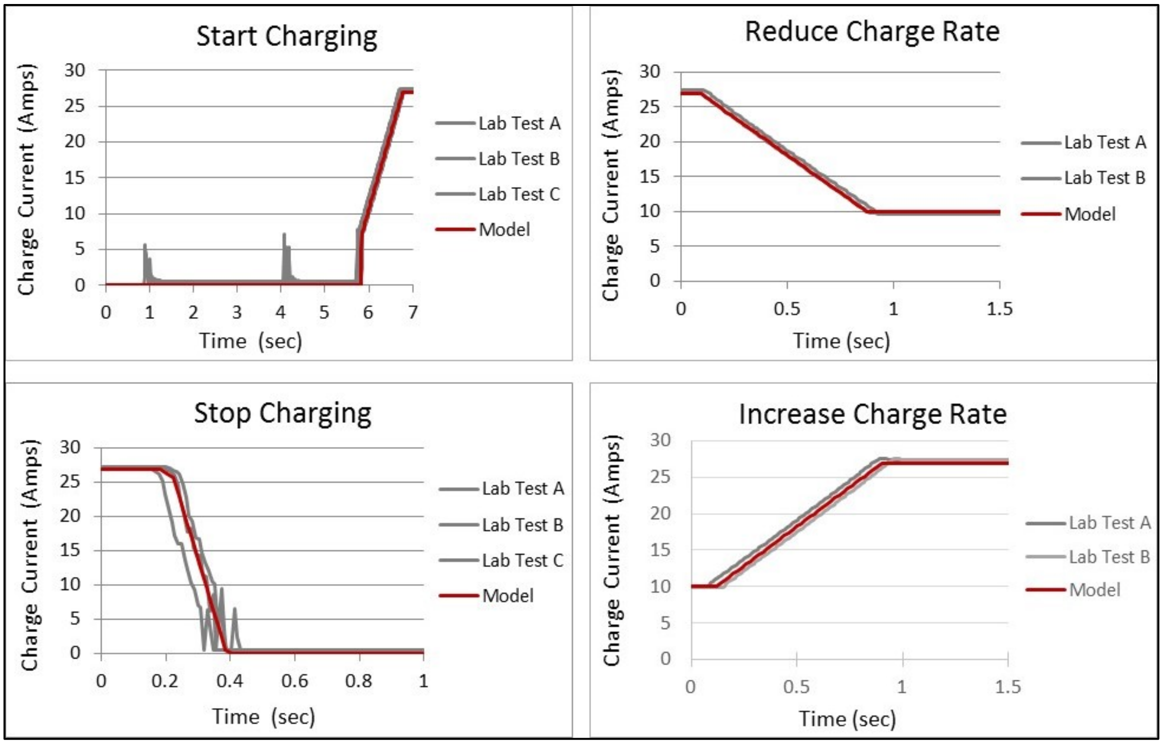

Figure 4. Comparison of laboratory test and model output results for a 2015 Nissan LEAF. The model output accurately represents the transitions from one charge rate to another charge rate.

2.1.2 Grid Impacts Simulation Environment

To understand how PEV charging might affect a distribution feeder and to develop and test PEV charging control strategies, it is important to have an accurate model of the distribution feeder system and non-PEV loads.

In the GM0085 Project residential simulation platform, the distribution feeder model is simulated in a Real Time Digital Simulator (RTDS). The RTDS provides a real-time environment for performing transient simulations and high-fidelity dynamic modeling of power components and systems. The distribution feeder system used is the IEEE 34 node test feeder (see Figure 5). This test feeder is characterized by a long and lightly loaded overhead transmission lines. It has a nominal voltage of 24.9 kV, two in-line regulators, one in-line transformer, and two shunt capacitors.

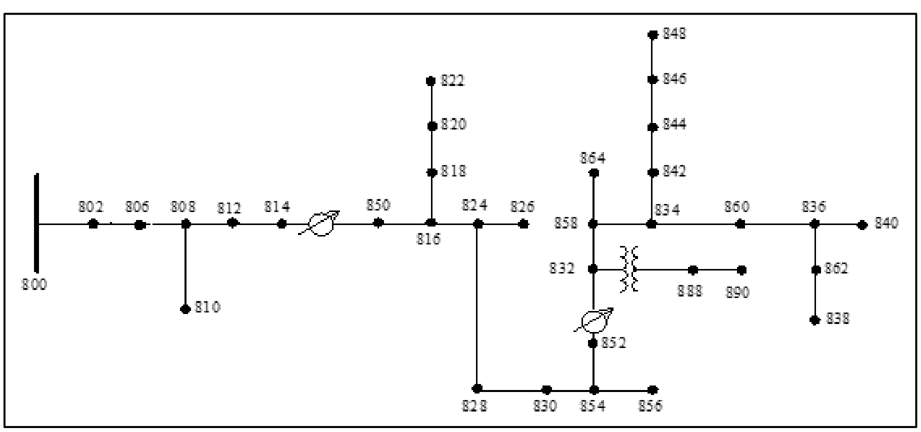

Figure 5. Schematic of IEEE 34 node test feeder.

The non-PEV feeder load profile used in the simulation environment is derived from the typical PG&E residential load profile downloaded from the PG&E website [5]. The typical residential load profile is an hourly load profile for each calendar year over a several year period and represents the typical or average load of a single residence in the PG&E service area. The non-PEV feeder load profile is calculated by multiplying the number of residences on the feeder by the typical residential load profile. The typical PG&E residential profiles were used to derive both the actual and forecasted non-PEV feeder load profiles. The actual profile used the PG&E data from July 27, 2016, and the forecasted profile used the PG&E data from the previous day, July 26, 2016. Both of these days are peak load days in the typical PG&E residential profile for 2016 (see Figure 6).

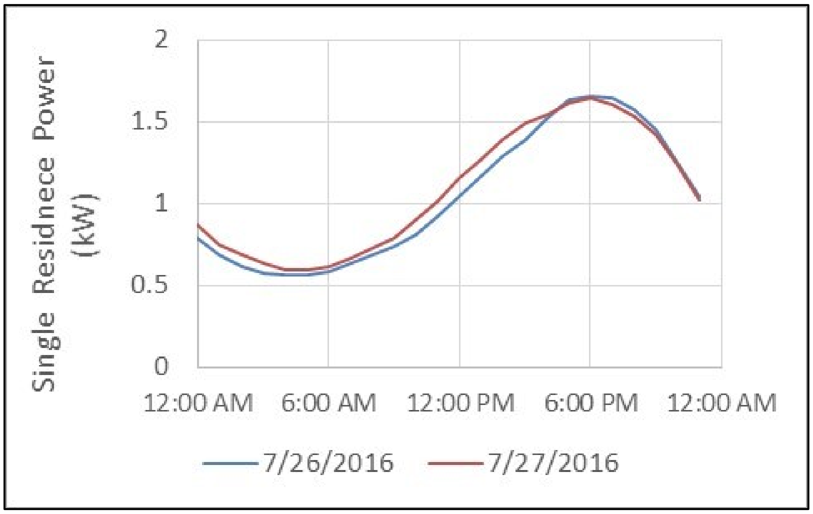

Figure 6. Typical or average load of a single residence in the PG&E area. The data on 7/27/2016 is used to calculate the actual feeder load profile; the data on the previous day, 7/26/2016, is used to calculate the forecasted feeder load profile.

2.2 Residential PEV Charging Control Strategy Description

The PEV charging control strategy developed in the GM0085 Project uses a centralized control element that will be referred to as the aggregator. The aggregator interacts with PEVs directly to determine the times during the day that each PEV should be charged. The aggregator functions in the "energy domain" by dividing each day into time segments and calculating the optimal amount of PEV charge energy for each time segment. In this report, each of these time segments are referred to as time steps. The aggregator's primary purpose is to ensure PEV charging needs are met and to meet grid objectives that require shifting PEV charge energy in time such as shifting PEV charging energy to off-peak load times.

The control strategy requires bi-directional communication between the aggregator and each PEV. This communication is summarized in the following steps and shown in Figure 7:

- Each PEV sends its charging needs to the aggregator
- The aggregator calculates an energy set point for each PEV for the next time step
- The aggregator sends an energy set point to each PEV

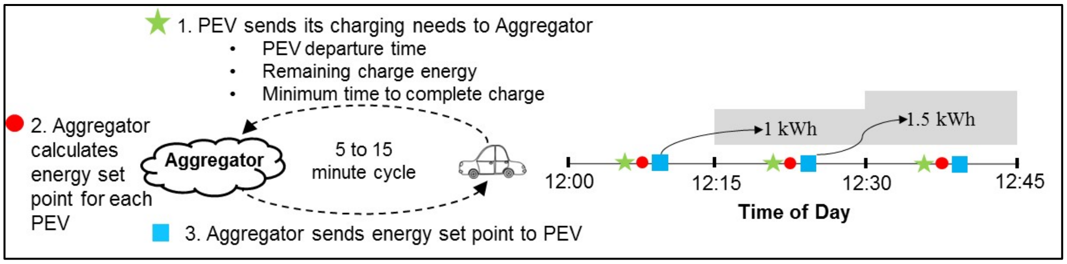

Figure 7. Bi-directional communication between the aggregator and each PEV occurs once every time step. In a given time step the aggregator calculates energy set points for each PEV for the next time step.

This communication sequence occurs every time step, allowing the aggregator to use the most recent PEV charging needs information. Since the communication sequence only occurs once every 5, 10, or 15 minutes, this strategy is not sensitive to internet latency and does not require low latency communication.

When designing the aggregator in the GM0085 Project, the dominant design criteria was scalability and computational efficiency. The aggregator needed to be able to calculate the energy set points for hundreds of thousands of PEVs on an ordinary personal computer in less than 1 minute. In order to achieve this, it became obvious early on that the optimization model could not represent individual PEVs. If each PEV is explicitly included in the optimization model, the number of decision variables is the product of the number of PEVs and the number of time steps in the prediction horizon. For example, as shown in *Equation (1)*, an optimization model including 300,000 PEVs with a prediction horizon of 24 hours and time step of 10 minutes would have 43.2 million decision variables. This is a very large optimization problem.

$$num\_PEVs = 300{,}000 \tag{1a}$$

$$num\_timesteps = \frac{prediction\ horizon\ duration}{time\ step\ duration} = \frac{24 * 60}{10} = 144 \tag{1b}$$

$$\begin{aligned} num\_decision\_variables &= num\_PEVs\ * num\_timesteps \\ &= 300{,}000 * 144 = 43.2\ million \end{aligned} \tag{1c}$$

The optimization problem can be made much smaller if the PEVs were represented collectively and not individually in the optimization model. When PEVs are represented collectively, their individual constraints are aggregated into a single set of constraints. Their individual energy set points over the prediction horizon are also aggregated into one set of aggregated energy set points. The number of decision variables in this type of reduced order optimization model does not depend on the number of PEVs. Rather, it is the number of time steps in the prediction horizon, which is 144 in the example shown in *Equation (1)*.

The GM0085 Project designed the aggregator to use an aggregation step followed by a reduced order optimization model followed by a disaggregation step. These steps are as follows:

1. Aggregate PEV constraints
2. Solve reduced order optimization model
3. Allocate energy to PEVs for the next time step

Steps 1 and 2 allocate the total PEV charge energy over the prediction horizon to meet some grid objective, such as shifting PEV charging to off-peak load times. Step 3 divides the total PEV charge energy for the next time step among the PEVs in a way to ensure that all PEV charging needs are met. Figure 8 shows this process.

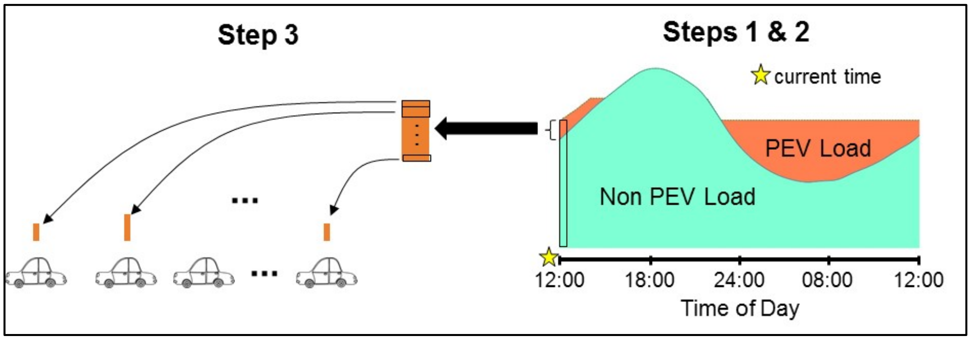

Figure 8. Control strategy allocates the total PEV load over the prediction horizon to minimize peak load (Steps 1 and 2). Step 3 divides the total PEV charge energy for the next time step among the PEVs in a way to ensure all PEV charging needs are met.

Figure 9 shows the data flow diagram for the aggregator. The data flow diagram includes the external environmental information the aggregator needs (in yellow boxes), as well as the three main analysis steps performed by the aggregator (in blue boxes). The external environmental information needed by the aggregator is as follows:

- Load forecast of the non-PEV load for the prediction horizon
- PEV charging needs forecast for the prediction horizon
- Charging needs of PEVs that are currently charging

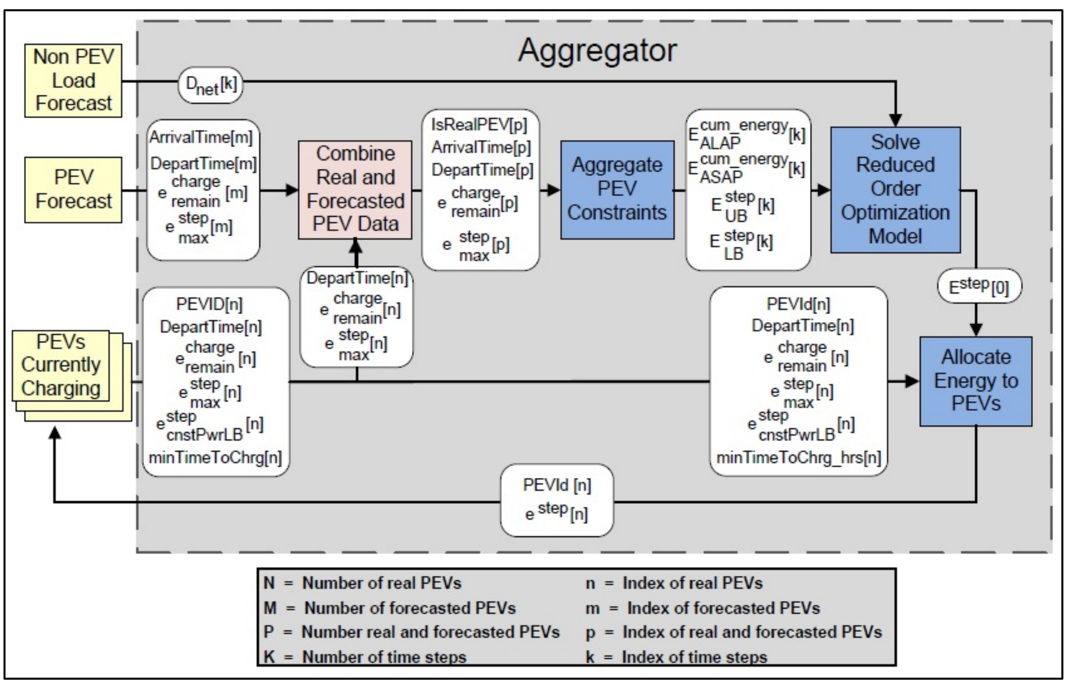

Figure 9. Aggregator data flow diagram. The three main analysis steps of the aggregator are displayed in the blue boxes. The external environmental information the aggregator needs is displayed in the yellow boxes. The information passed between functional blocks is displayed in the white boxes.

The creation of accurate non-PEV load forecasts and PEV charging needs forecasts was not the focus of the GM0085 Project. When developing, debugging, and testing the control strategy, the GM0085 Project generated these forecasts by adding randomness into available historical data. Ref. [4] describes the creation of PEV charging needs from historical PEV charging data. The three analysis steps performed by the aggregator are described in Sections 2.2.1, 2.2.2, and 2.2.3.

2.2.1 Aggregate PEV Constraints

Combining individual PEV charging constraints into a single aggregate set of charging constraints is the key insight that enabled the GM0085 Project to calculate energy set points for hundreds of thousands of PEVs on a personal computer in less than 1 minute. Aggregating PEV charging constraints transforms a potentially huge optimization problem into a reduced order optimization problem that is small and easy to solve quickly with minimal computational resources.

It is not possible for PEVs to charge faster than their maximum charge rate or to charge at times when they are not connected to a charger. In order to enforce these conditions, all valid PEV charging is bound by "as soon as possible" (ASAP) charging and "as late as possible" (ALAP) charging (see Figure 10). ASAP charging occurs when the PEV immediately starts charging as soon as it is connected to a charger and continues to charge until the PEV's charging needs are met. ALAP charging occurs when the PEV waits until the last minute to begin charging and the PEV's charge needs are met just before the PEV is scheduled to depart.

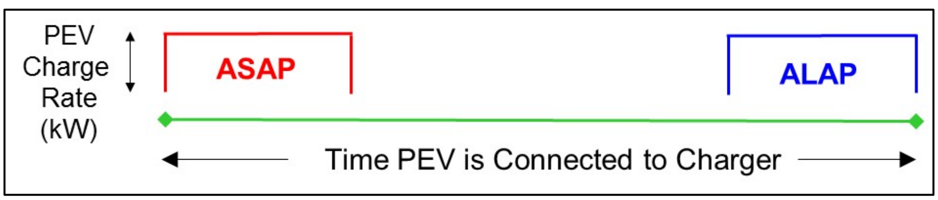

Figure 10. All PEV charging is bound by ASAP and ALAP charging. ASAP charging is when the PEV is charged as soon as possible. ALAP charging is when the PEV is charged as late as possible.

There are two types of aggregate PEV constraints used in the reduced order optimization model, cumulative energy constraints and step energy constraints.

Cumulative energy constraints are calculated for both ASAP charging and ALAP charging. ASAP charging corresponds to an upper bound and ALAP charging corresponds to a lower bound. These cumulative energy constraints ensure that the energy the aggregator allocates through time is sufficient to meet the charging needs of all PEVs. A point above the cumulative energy upper bound corresponds to a scenario where the aggregator is attempting to charge PEVs before they are connected to a charger or at a charge rate that is too large. A point below the cumulative energy lower bound corresponds to a scenario where the aggregator is attempting to charge PEVs after they have departed. The aggregator's cumulative energy being bound by the cumulative energy constraints is a necessary but not a sufficient condition to ensure all PEV charging needs are met. To ensure all PEV charging needs are met, it is also necessary to prioritize which PEVs can charge based upon the remaining time each PEV can charge and the remaining energy required. The project used two types of aggregate PEV constraints in the reduced order optimization model, cumulative energy constraints and step energy constraints. This is discussed further in Section 2.2.3.

The manner in which ASAP and ALAP cumulative energy constraints are calculated is identical. The only difference is whether ASAP charging or ALAP charging is used in the calculation. A cumulative energy constraint is the sum of the cumulative energies of all PEVs as shown in *Equation (2)*. *Equation (3)* shows how to calculate the cumulative energy for a single PEV.

$$k\_start[n] \rightarrow \text{The time step k when PEV n started charging}$$
$$k\_end[n] \rightarrow \text{The time step k when PEV n finished charging}$$
$$e^{step}[n,z] \rightarrow \text{The energy set point for PEV n at time step z}$$
$$e^{cum}[n,k] \rightarrow \text{The cumulative energy for PEV n at time step k}$$
$$E^{cum}[k] \rightarrow \text{The cumulative energy of all PEVs at time step k}$$

$$E^{cum}[k] = \sum_{n=1}^{N} e^{cum}[n,k] \tag{2}$$

$$e^{cum}[n,k] = \begin{cases} 0 & k < k\_start[n] \\ \displaystyle\sum_{z=k\_start[n]}^{k} e^{step}[n,z] & k\_start[n] \le k \le k\_end[n] \\ \displaystyle\sum_{z=k\_start[n]}^{k\_end[n]} e^{step}[n,z] & k > k\_end[n] \end{cases} \tag{3}$$

Figure 11 shows a graphical representation of the cumulative energy constraints for two hypothetical PEVs. Notice that the cumulative energy of PEV 1 and PEV 2 will always be bound by the ASAP and ALAP cumulative energy constraints when the charging is valid. Valid charging consists of two bounding criteria, first that PEVs are only allowed to charge when they are connected to a charger, and second that a PEV's charge rate never exceeds its maximum charge rate.

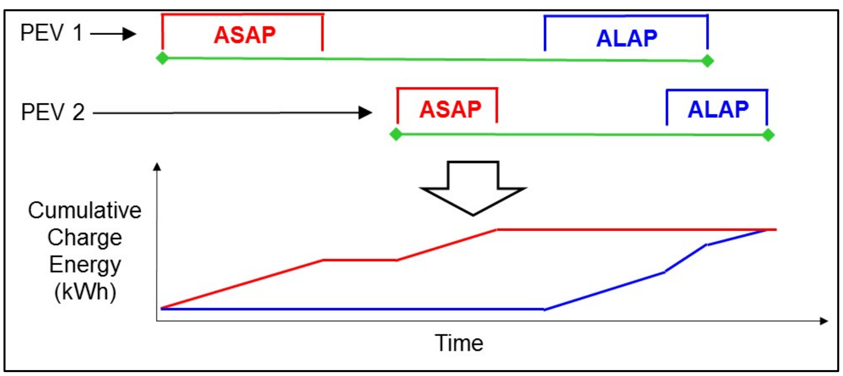

Figure 11. Graphical representation of the ASAP and ALAP cumulative energy constraints for two PEVs. All valid PEV charging for PEV 1 and PEV 2 is bound by the ASAP and ALAP cumulative energy constraints.

Unlike cumulative energy, which is the total energy drawn by all PEVs from the beginning of their respective charges up to the present time step, step energy is the total energy drawn by all PEVs during a given time step and is the decision variable of the optimization model. The step energy upper bound and lower bound constraints are intended to constrain the total energy the aggregator can allocate to the PEVs during individual time steps. The step energy lower bound is always zero since this control strategy was designed for grid to vehicle charging only. The step energy upper bound for a given time step is the maximum amount of energy that all PEVs can collectively draw during that time step (*Equation (4)*). It is important to note that the maximum step energy for a given PEV is zero when the PEV's charging needs have been met or its battery is full, since the PEV does not require any more energy. As a result, the step energy upper bound at a given time step depends on the step energy values of the previous time steps.

This creates the undesirable situation where one of the constraints of the reduced order optimization model (step energy upper bound) depends on the decision variable (step energy). This is the trade-off of the reduced order optimization model, which provides a huge reduction in the size of the optimization problem at the expense of making one of the constraints in the optimization model dependent on the decision variable.

$E_{UB}^{step}[k] \rightarrow$ The step energy upper bound at time step k

$e_{max}^{step}[n,k] \rightarrow$ The max energy PEV n can draw at time step k

$$E_{UB}^{step}[k] = \sum_{n=1}^{N} e_{max}^{step}[n,k] \tag{4}$$

In the GM0085 Project, the step energy upper bound was calculated under the assumption that PEVs would be able to draw maximum power from the grid the entire time they were connected to a charger (see Figure 12). This simplifying assumption makes sub-optimal PEV charging a possibility. As will be shown in Section 2.3, this control strategy works extremely well for residential charging. Even though the simplifying assumption works well for residential charging it may be problematic in other charging situations. This is an area where future work is needed both to investigate non-residential charging scenarios, as well as to determine if there are better ways to estimate the step energy upper bound constraint.

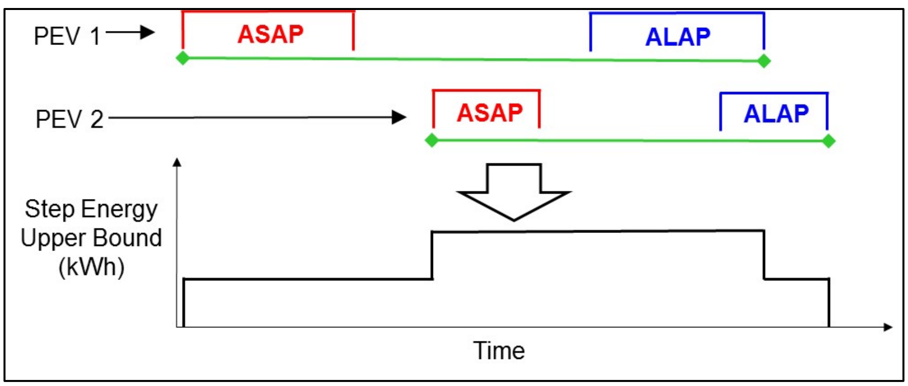

Figure 12. Graphical representation of the step energy upper bound for two hypothetical PEVs. The step energy upper bound was calculated under the simplifying assumption that PEVs would be able to draw maximum power from the grid the entire time they were connected to a charger (ALAP charging).

2.2.2 Solve Reduced Order Optimization Model

The reduced order optimization model is specified in *Equation (5)* and a graphical example of the step energy and cumulative energy constraints is shown in Figure 13. The optimization model decision variable, $E^{step}[k]$, is the step energy for every time step in the prediction horizon. The objective function in *Equation (5a)* allocates the step energy (PEV load) so that the total load (sum of PEV and non-PEV loads) has the smallest possible peak and is as flat as possible.

The optimization model also has three sets of constraints:

1. Constraints in *Equation (5b)* ensure that the cumulative energy of the optimized solution is bound by the cumulative energy constraints.
2. Constraints in *Equation (5c)* ensure that the step energy is bound by the step energy constraints.
3. Constraints in *Equation (5d)* ensure that the total energy (sum of PEV and non-PEV energy) does not exceed the maximum energy the feeder can supply in a single time step.

$E_{ALAP}^{cum}[k] \rightarrow$ The ALAP cumulative energy constraint

$E_{ASAP}^{cum}[k] \rightarrow$ The ASAP cumulative energy constraint

$E_{LB}^{step}[k] \rightarrow$ The step energy lower bound constraint

$E_{UB}^{step}[k] \rightarrow$ The step energy upper bound constraint

$E^{step}[k] \rightarrow$ The step energy (**Decision Variable**)

$D_{net}[k] \rightarrow$ The load forecast of the non PEV load

$Feeder_{limit}^{step} \rightarrow$ The max energy the feeder can supply

$k \rightarrow$ The index of the time step

$$min \sum_{k=1}^{K} (E^{step}[k] + D_{net}[k])^2 \qquad (5a)$$

$$s.t. \quad E_{ALAP}^{cum}[k] \leq \sum_{z=1}^{k} E^{step}[z] \leq E_{ASAP}^{cum}[k] \qquad (5b)$$

$$0 = E_{LB}^{step}[k] \leq E^{step}[k] \leq E_{UB}^{step}[k] \qquad (5c)$$

$$E^{step}[k] + D_{net}[k] \leq Feeder_{limit}^{step} \qquad (5d)$$

$$k = 1,2,\ldots,K$$

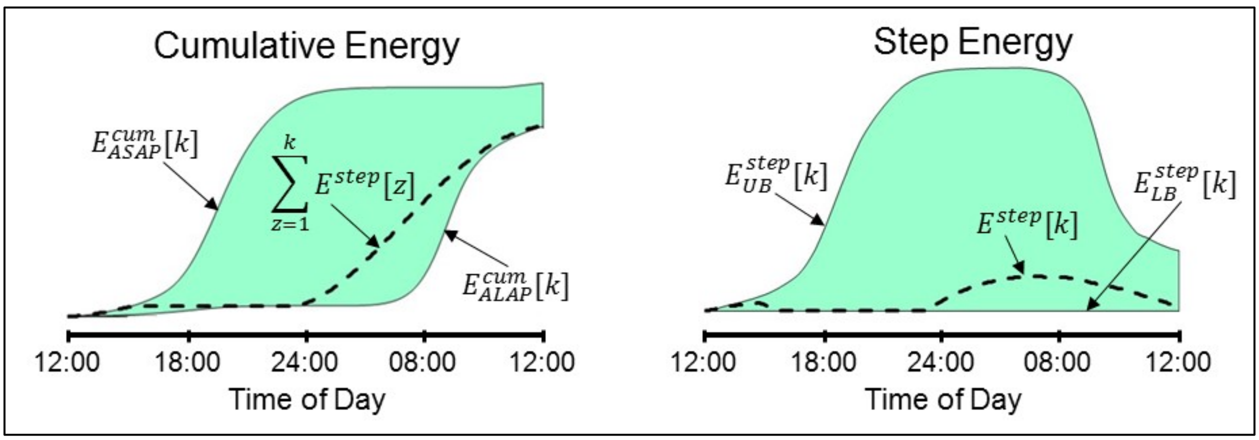

Figure 13. Hypothetical graphical representation of the cumulative energy constraints, the step energy constraints, and an optimized E^{step}[k] for a 24-hour prediction horizon.

2.2.3 Allocate Energy to PEVs

Allocating energy to an individual PEV is a disaggregation step that divides $E^{step}[0]$, the total PEV charge energy for the next time step, among the PEVs in a way to ensure all PEV charging needs are met. A calculated value called the charge priority is used to determine which PEVs should charge. The charge priority is a PEV's minimum remaining charge time divided by its remaining park time as shown in *Equation (6)*. A PEV's minimum remaining charge time is the time required for the PEV's charging needs to be met when the PEV is charged at its maximum charge rate. A PEV's remaining park time is the time until the PEV departs.

$$charge\ priority[k] = \frac{minimum\ remaining\ charge\ time[k]}{remaining\ park\ time[k]} \qquad (6)$$

Charge priority is an indication of urgency to charge. For example, a charge priority of 0.9 indicates that the PEV must charge at its maximum charge rate for 90% of the remaining park time to meet its charging needs, whereas a charge priority of 0.10 indicates that only 10% of the remaining park time is required to fully charge the PEV. Stated another way, a charge priority of 0.9 indicates that the PEV must charge at 90% of its maximum charge rate for all the remaining park time, and a charge priority of 0.10

indicates that the PEV must be charged at only 10% of the maximum charge rate for the remaining park time to fully charge the PEV.

After charge priority has been calculated for all PEVs, charge energy is allocated to each PEV in descending order of charge priority. Allocating energy in this way gives a PEV with higher charge priority charge energy before a PEV with lower charge priority. Once the total energy allocated to the PEVs is equal to $E^{step}[0]$, then all remaining PEVs are given an energy set point value of zero.

Allocating energy to the PEVs in descending order of charge priority is a necessary, but not a. sufficient condition to ensure their charging needs are met. It is also necessary that the PEV energy set points are large enough to meet their charging needs. The control strategy accomplishes this by allocating energy to each PEV in the range specified by *Equation (12)*.

$e^{step}[k] \rightarrow$ The energy set point for the PEV at time step k
$e^{step}_{max}[k] \rightarrow$ The max energy the PEV can draw at time step k
$MRCT[k] \rightarrow$ The minimum remaining charge time at time step k

$$MRCT[k+1] = MRCT[k] - \frac{e^{step}[k]}{e^{step}_{max}[k]} * aggregator\ time\ step \quad (7)$$

$$e^{step}_{LB}[k] = charge\ priority[k] * e^{step}_{max}[k] \quad (8)$$

$$e^{step}[k] < e^{step}_{LB}[k] \rightarrow charge\ priority[k+1] > charge\ priority[k] \quad (9)$$

$$e^{step}[k] = e^{step}_{LB}[k] \rightarrow charge\ priority[k+1] = charge\ priority[k] \quad (10)$$

$$e^{step}[k] > e^{step}_{LB}[k] \rightarrow charge\ priority[k+1] < charge\ priority[k] \quad (11)$$

$$charge\ priority[0] * e^{step}_{max}[0] < e^{step}[0] \leq e^{step}_{max}[0] \quad (12)$$

The lower bound in *Equation (12)*, which is also given in *Equation (8)*, defines the energy set point that will cause the charge priority to remain constant. As shown in *Equation (9)* and *Equation (11)*, whenever the energy set point is less than e^{step}_{LB}, the charge priority will increase, and whenever the energy set point is greater than e^{step}_{LB}, the charge priority will decrease. A consequence of this control strategy is that a PEVs charge priority decreases when it is charged and increases when it is not charged. The minimum remaining charge time as a function of the energy set point is given in *Equation (7)*.

2.3 Residential Control Strategy Results

The platform described in Section 2.1 was used to investigate the benefit of the PEV charging control strategy described in Section 2.2. In the simulation there were 75,000 homes on the distribution feeder where 50% of the homes owned a PEV. In these simulations, the residential charging control strategy was shown to provide grid services. The grid services that were provided were voltage support and capacity deferral that are described in Sections 2.3.1 and 2.3.2, respectively.

2.3.1 Voltage Support

When PEV charging is controlled, the voltage profile on the feeder is considerably flatter. Figure 14 shows the voltage profiles for Node A and Node B on the IEEE 34 node test feeder. Figure 15 shows the location of these two nodes on the feeder. Node A is closer to the feeder substation than Node B causing Node A to have less variation in the voltage profile than Node B. When the charging is not controlled, the voltage deviates outside the normally accepted limits (±5% of nominal). By contrast, when charging is controlled, the voltage is always within the normally accepted limits. This is significant since the need for infrastructure investment to maintain feeder voltage as the PEV penetration increases is reduced.

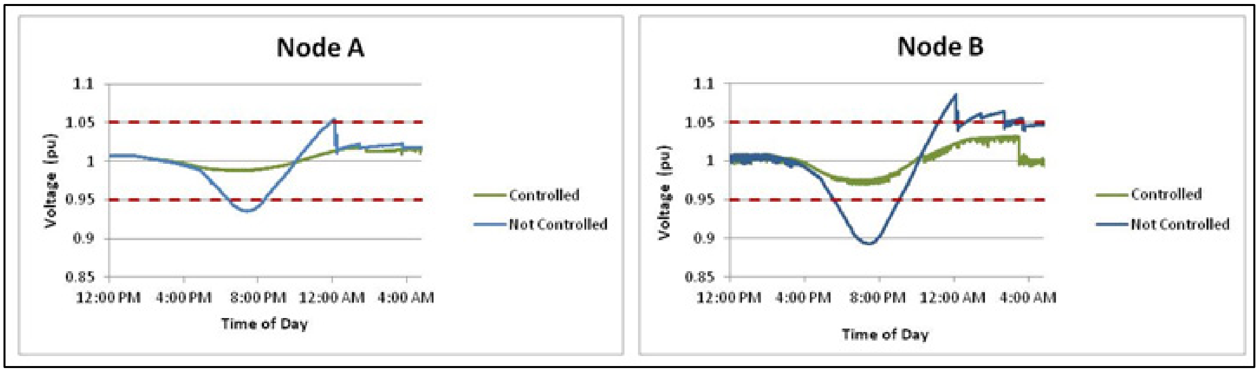

Figure 14. Voltage profile at Node A and Node B when PEV charging is controlled and not controlled. The range of acceptable voltage magnitudes (±5% of nominal) is indicated between the dashed red lines.

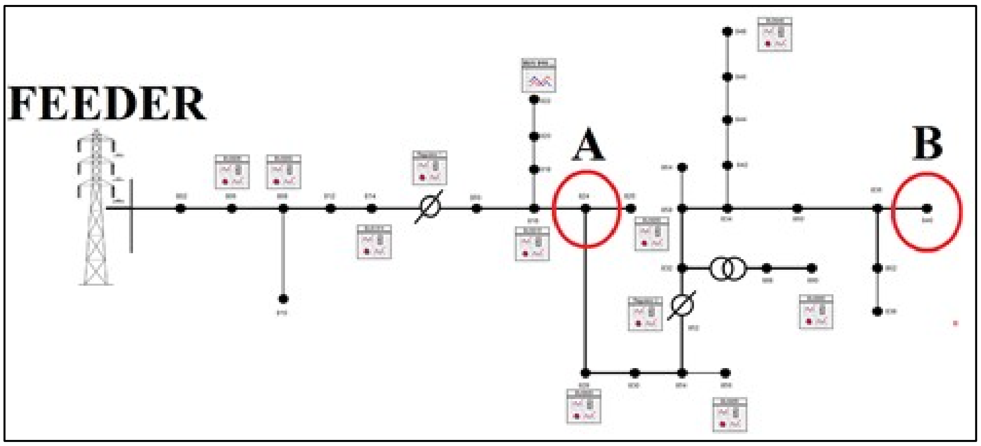

Figure 15. Location of Node A and Node B on the IEEE 34 node test feeder.

2.3.2 Capacity Deferral

The residential control strategy is able to provide significant capacity deferral. Figure 16 shows the feeder load profiles when there are no PEVs charging, when the PEV charging is not controlled, and when the PEV charging is controlled using the residential control strategy. When charging is not controlled, each PEV begins charging as soon as it is connected to a charger and continues to charge as fast as possible until its charge is complete. When PEV charging is not controlled, the PEV charging occurs at the same time as the peak of the non-PEV load. This increases both the peak and ramping in the feeder load when compared to the feeder load with no PEV charging. By contrast, controlled charging shifts the PEV charging to off-peak hours, which flattens the feeder load profile and causes only a very small increase in peak load. Controlled charging in large part mitigates the need for capacity upgrades to residential feeders as PEV penetration increases.

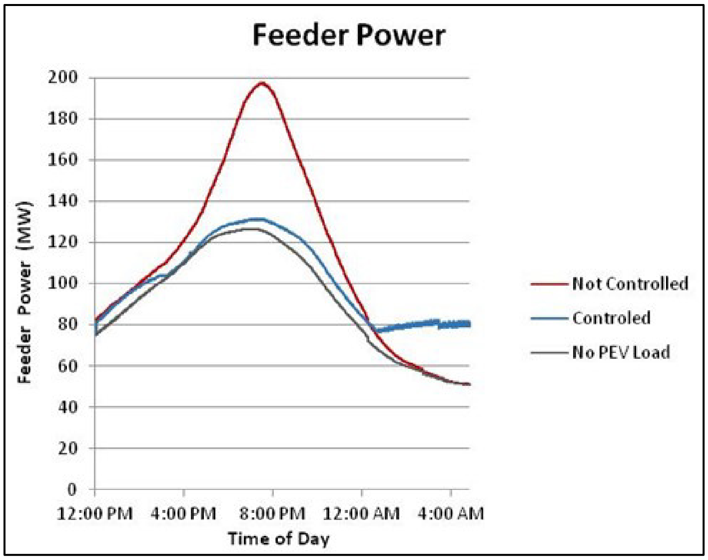

Figure 16. Feeder load profile when there are no PEVs are charging, when PEV charging is not controlled, and when PEV charging is controlled.

The peak feeder loads for the scenarios are as follows:

- 127 MW: No PEV charging
- 132 MW: Controlled PEV charging
- 197 MW: Uncontrolled PEV charging

Stated another way, controlled charging requires a 4% increase in capacity, whereas uncontrolled charging requires a 55% increase in capacity.

2.3.3 Benefit of Capacity Deferral

As PEVs directly increase the peak demand on the grid, they reduce the capacity margin planned by utilities. We propose to quantify the number of years lost before new investments need to be made to increase capacity margin. The cost of those investments is complex to find. Utilities regularly need to estimate the overall cost for distribution grid upgrades, for instance to define retail rates for their customers. However, the team does not have enough data, nor the utility knowledge to estimate the cost of a system reinforcement. Instead, we propose to give results in term of years of lost load growth, which can be used by utilities to estimate the costs for individual feeders.

We first illustrate the methodology behind the estimation of years of lost load growth with a feeder in Santa Rosa, California [6]. The feeder has a current peak demand of 9.2 MW and a maximum capacity of 12.2 MW. The feeder is providing energy to 5,533 residential customers, which have on average 1.87 vehicles (Census survey from 2015 and 2016). Furthermore, the EV growth shown in Figure 17 allows us to estimate the number of EVs on that feeder for each year (details are provided in Appendix A). From the information above and the assumption of a natural 1.1% increase in peak demand per year [7], a peak increase of 1.5 kW per uncontrolled EVs and a peak increase of 0.047 kW per controlled EVs (as addressed in Section 2.3.2). We calculate peak demand growth for three scenarios, no EVs, uncontrolled EVs, and controlled EVs. From this example, we can see that the few uncontrolled EVs in 2020 lead to the same peak demand increase as would the natural peak demand growth in 2030 (black dashed line in Figure 18); therefore, in 2020, uncontrolled EVs would have caused 10 years of lost load growth. Note that in the uncontrolled scenario, EVs are using all the feeder's remaining capacity as soon as 2023 (red dashed line in Figure 18).

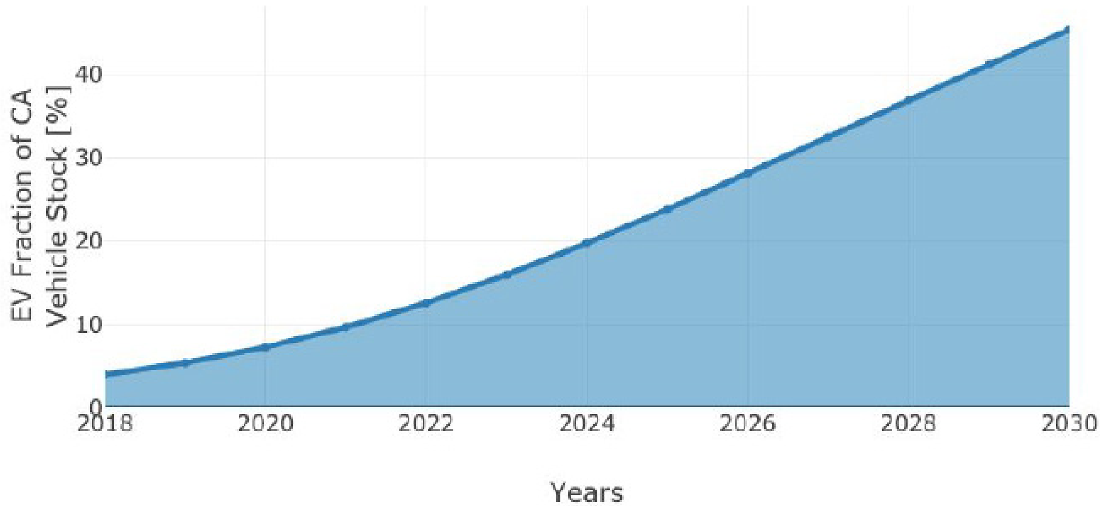

Figure 17. Projection of EVs in the total vehicle stock in California (see Appendix A).

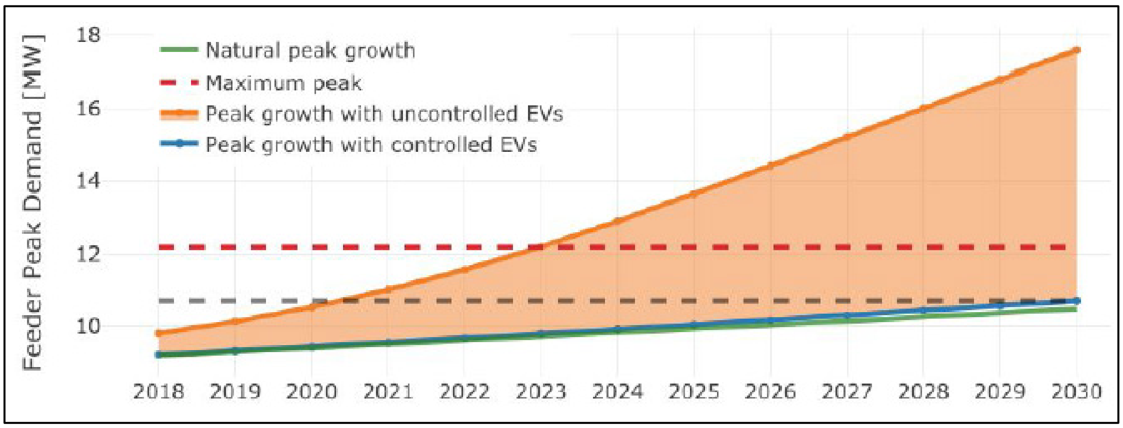

Figure 18. Peak demand increase for feeder "MONROE 1106" with uncontrolled PEVs (orange) and controlled PEVs (blue). The black dashed line represents the peak increase from natural growth in 2030. The red dashed line represents the feeder's maximum allowed peak demand.

We generalize our results for a residential feeder with a 10 MW peak demand. We consider that households drive the peak demand by consuming on average 1.6 kW on-peak; furthermore, we assume two vehicles per households. Note that certain residential feeders might have less households because their peak demand is not entirely driven by households, but also by commercial and industrial loads.

In this analysis, we give the number of years needed for a 1.1% natural peak demand growth to match the 1.5 kW peak demand increase per uncontrolled EVs and 0.047 kW per controlled EVs. We find that by 2030 uncontrolled EVs could lead to more than 50 years of lost load growth for typical residential feeders (see Figure 19). By contrast when PEV charging is controlled there will be just a little over one year of lost load growth in 2030. This means that the capacity margin that utilities may expect to accommodate future load growth for the next 10, 20, or 30 years will not be affected when PEV charging is controlled, but may be used up by uncontrolled PEV charging in a couple of years requiring distribution system upgrades much sooner than anticipated.

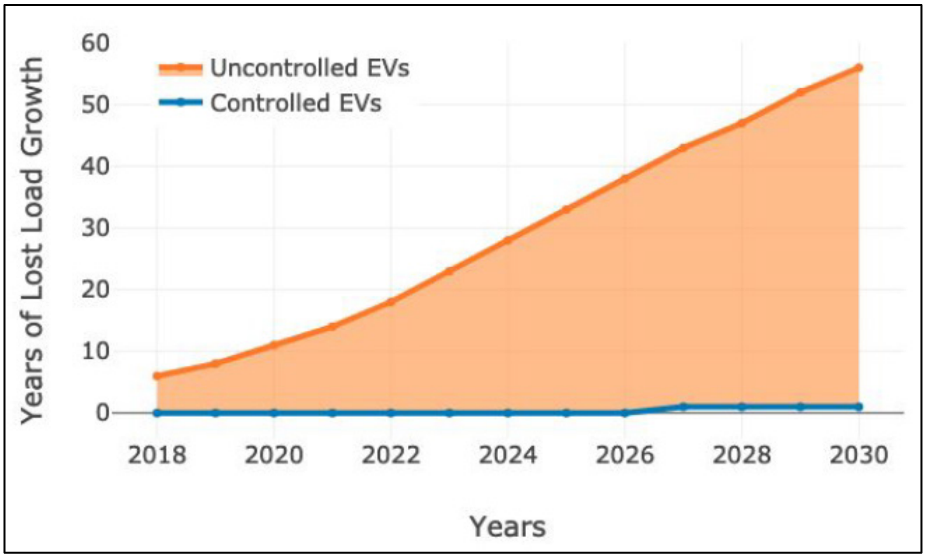

Figure 19. Years of lost load growth as a function of calendar years for a typical residential distribution grid with a 10 MW peak demand.

2.3.4 Computational Performance

When designing the residential control strategy, the dominant design criteria was scalability and computational efficiency. The control strategy needed to be able to calculate the energy set points for hundreds of thousands of PEVs on an ordinary PC in less than 1 minute. Figure 20 shows the execution times during a day for PEV populations of 50,000, 100,000, 250,000, and 500,000. From Figure 20, we can see that the maximum computation time for 500,000 is a little over 4 seconds. This shows that this control strategy is very computationally efficient. Simulations are conducted on the demonstration platform by using a Linux desktop with the following specifications: Intel CPU Core 2 Duo E8400 with 3G HZ and 14.6 GB memory.

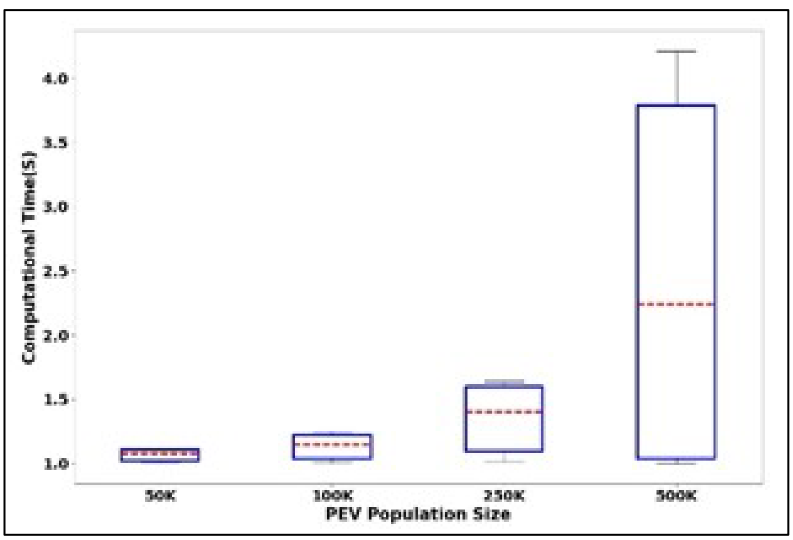

Figure 20. Residential control strategy computation times for PEV populations of 50,000, 100,000, 250,000, and 500,000.

3. RESEARCH OF PEV CHARGING AT COMMERCIAL BUILDINGS

3.1 Overview

The objective of this project is to understand the grid services potential and assess the impacts of multiple commercial buildings where PEVs are charging that are connected to a distribution feeder. This project has developed a model for an aggregator that acts as an intermediary between the utility and commercial buildings with building energy management systems (BEMSs) that locally control PEV charging. The aggregator model is built to interface with the real-time hardware-in-the-loop platform and to communicate with each building and coordinate the buildings' responses across the distribution feeder.

The aggregator is located at Idaho National Laboratory (INL) to communicate with buildings located at Argonne National Laboratory (ANL), National Renewable Energy Laboratory (NREL), and Pacific Northwest National Laboratory (PNNL) where actual PEVs are charging. The control for these buildings was developed in the GM0062 Project and integrates the PEV charging at each location into the building load. The buildings aggregator is used to communicate with buildings and coordinate their response across a distribution feeder to achieve a grid objective or provide a grid service. It is the building that decides whether or not to participate and the building ultimately decides how to manage its energy consumption. The aggregator only calculates a request for buildings that have indicated availability to participate, and the request must fall within parameters provided by the building based on the total building load. The building provides these parameters, or limits, based on its own determination of whether it should shed (or possibly increase) the PEV charging load to maintain the appropriate overall load. The impact on the distribution feeder of PEV charging controlled by commercial buildings, with and without aggregator support, has been studied in a real-time environment with hardware in loop (HIL) capabilities at INL. This platform will interact with the aggregator and the building loads at ANL, NREL, and PNNL to understand the grid impacts of widespread PEV charging, as well as the value of the aggregator.

3.2 Commercial Control Testing/Development Platform

Multi-laboratory platform for development and testing of aggregator-assisted control of PEV charging at commercial buildings is displayed in Figure 21. This platform consist of a MQTT central broker described in Section 3.2.1, a DRTS described in Section 3.2.2, and an aggregator described in Section 3.3. The building level controls implemented at buildings located at ANL, PNNL, and NREL are each described in Section 3.4.

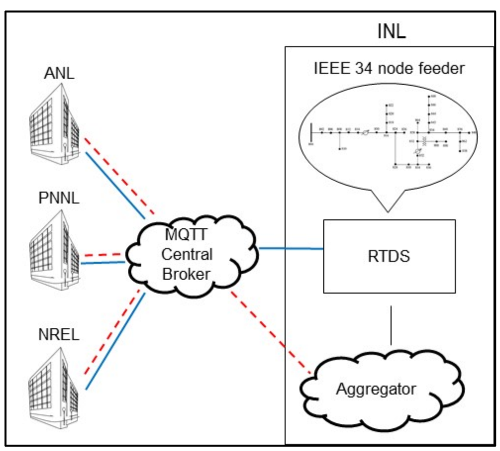

Figure 21. Multi-laboratory platform for development and testing of aggregator-assisted control of PEV charging at commercial buildings.

3.2.1 GM0085 MQTT Central Broker

Message Queuing Telemetry Transport (MQTT) is a lightweight message transport protocol in which an MQTT broker (server) facilitates messaging between clients. MQTT is becoming the de-facto standard for Internet of Things (IoT) communication and is an OASIS standard. MQTT is based on a publish and subscribe model in which clients can subscribe or publish to individual topics. MQTT topic structure is similar to a personal computer's directory structure with folders and subfolders. An example topic for the GM0085 is: DOE/GM0085/ANL/Setpoint, which is the set point for ANL's building published by the INL aggregator.

ANL utilizes MQTT in their open-source common integration platform (CIP.io) and sets up secure MQTT brokers and MQTT clients. For the GM0085 MQTT central broker, ANL used the open-source Mosquitto broker. The broker was hosted on an Amazon EC2 Ubuntu server instance. Each laboratory was provided credentials for authorization and access control lists were used to limit read/write access to specific GM0085 topics. In addition, all communication was encrypted using TLS v1.2.

The broker provided sub-second communication latency between INL, ANL, NREL, and PNNL to enable interlaboratory communication to perform the GM0085 hardware in the loop research.

3.2.2 Digital Real-time Simulator

The IEEE 34 bus distribution system model (see Figure 22) is enhanced to represent the real-time PG&E grid characteristics. The original system is 60-Hz, 24.9-kV, and 12-MVA system with various fixed and distributed loads. In this enhanced system, the generator is tuned to emulate the PG&E source. The building loads from ANL, NREL, and PNNL are modeled as dynamic loads that are controllable. The PG&E load is also modeled as dynamic load that is uncontrollable. Figure 22 shows the building loads positioned beside each other to observe the maximum impact of these loads on the grid.

The PG&E load and building loads in the DRTS are fed from the MQTT broker through a GTNET socket. The GTNET socket in the DRTS uses User Datagram Protocol (UDP) communication to communicate with the MQTT broker.

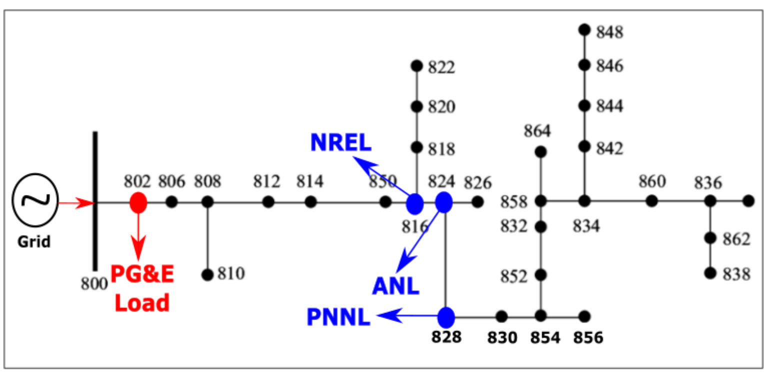

Figure 22. IEEE 34 bus distribution system model.

3.3 Building Aggregator

The aggregator built in this project acts as an intermediary between the utility and commercial buildings with BEMSs that locally control PEV charging (see Figure 23). The aggregator communicates with each building via the MQTT central broker and coordinates the buildings' responses across the distribution feeder. The aggregator is hosted at INL and contains an optimization routine to mitigate the negative grid impact from the building energy demand. At a high level, the communication between the aggregator and buildings is as follows:

- Three buildings at ANL, NREL, and PNNL, respectively, send the energy limits forecast (forecasted minimum energy and maximum energy) in a specified time horizon to the aggregator at INL every 10 minutes.
- The aggregator determines the optimal energy request of the next time step for each building using the received forecasted energy limits based on the defined optimization routine.
- Each building responds the aggregator set point based on their locally PEV charging control for every 10-minute interval.

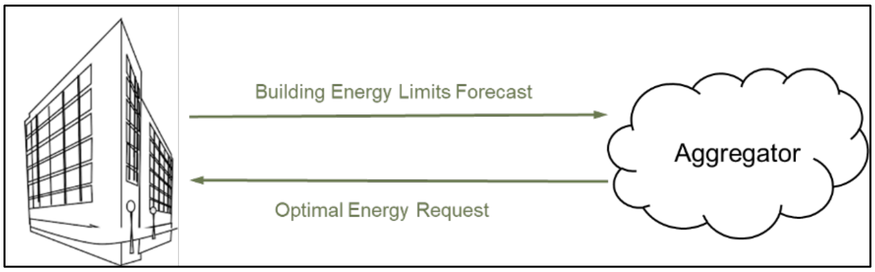

Figure 23. Communication information flow between buildings and the aggregator.

Each building forecasted maximum and minimum energies for the next hour broken up by 10-minute intervals and the following 5 hours broken down by hours. Each building will publish to these forecasted energy limits using MQTT on a 10-minute interval. An energy set point published by the aggregator for each building is the allocated energy for each building in the next 10 minutes.

Suppose in total B buildings are involved into the aggregator control (e.g., $B = 3$ in this specific study). For each building with index $b = 1, \dots, B$, we have the forecasted energy information at time step i: minimum energy $E_{min}^{b}[i]$ and maximum energy $E_{max}^{b}[i]$, where $i = 0, \dots, N-1$. N is the overall number of forecasted time steps in the prediction horizon. In the current implemented system, we have $N = 11$. When $i = 0, \dots, 5$: energy limits information is for a 10-minutes interval in the next first hour. When $i = 6, \dots, 10$: energy limits information is for one-hour interval in the following 5 hours.

The decision-making process in the building aggregator is a multi-step optimization routine, which is a low computational complexity optimization routine in order to be extendable for future large-scale control scenarios. In general, it includes three main modules, energy constraints aggregation, optimization routine, and building energy allocation (see Figure 24). Details related to each module are provided in Section 3.3.1.

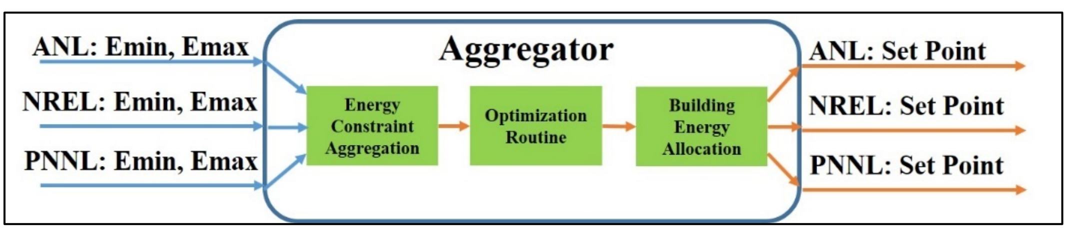

Figure 24. Optimization routine and framework for the aggregator.

3.3.1 Aggregator Decision-making Modules

3.3.1.1 Energy Constraints Aggregation

The energy constraints include both the lower bound and upper bound. The aggregated lower bound of energy constraint $E_{LB}^{step}[i]$ at forecasted time step i is the summation of minimum energy requirements from buildings. The aggregated upper bound of the energy constraint $E_{UB}^{step}[i]$ at forecasted time step i is the summation of maximum energy requirements from buildings. The mathematical equations are as follows:

$$E_{LB}^{step}[i] = \sum_{b=1}^{B} E_{min}^{b}[i] \tag{13}$$

$$E_{UB}^{step}[i] = \sum_{b=1}^{B} E_{max}^{b}[i] \tag{14}$$

3.3.1.2 Optimization Model

The optimization model aims to mitigate the negative impact on the grid from the building energy demand. The specific target or optimization purposes are determined by the objective function $f(E^{step}[\mathrm{i}])$. The objective functions will be defined for different control scenarios.

$$min\ \ f(E^{step}[i]) \tag{15a}$$

$$s.t. E_{LB}^{step}[i] \le E^{step}[i] \le E_{UB}^{step}[i] \tag{15b}$$

$$E^{step}[\mathrm{i}] + D_{net}[\mathrm{i}] \le Feeder_{EnrgyLmt}^{step} \tag{15c}$$

$$i = 0, \dots, N-1 \tag{15d}$$

In the optimization model, decision variable $E^{step}[\mathrm{i}]$ is the overall energy to be allocated at following time step i for all involved buildings. $E_{LB}^{step}[i]$ and $E_{UB}^{step}[i]$ are the aggregated lower bound and upper bound for building energy at time step i, respectively. $D_{net}[\mathrm{i}]$ is the uncontrollable commercial load on the feeder. $Feeder_{EnrgyLmt}^{step}$ is the corresponding feeder limit. According to the defined data format in this project, the received energy data array from each building has two different time scale. For both the forecasted minimum and maximum energy information, first six data points are the energy values during 10-min time interval, the following five data points are the energy values during 1-hour time interval. In order to improve the stability of the optimization process, it may be better to transform the five 1-hour data points to the corresponding thirty 10-minute data points by using the average values. This operation ensures all decision variables to have in the same scale in the optimization models and achieve a better performance of decision making. Therefore, in all we have N=6+5*6=36 decision variables.

The control target is determined by the selection of objective function in the optimization model. The following are two specific examples of optimization objectives for two different targets:

1. Reduce ramping:

$$f(E^{step}[\mathrm{i}]) = \sum_{i=1}^{N-1} ((E^{step}[\mathrm{i}] + D_{net}[\mathrm{i}]) - (E^{step}[\mathrm{i}-1] + D_{net}[\mathrm{i}-1]))^2 \tag{16}$$

2. Capacity deferral:

$$f(E^{step}[\mathrm{i}]) = \sum_{i=0}^{N-1} (E^{step}[\mathrm{i}] + D_{net}[\mathrm{i}])^2 \tag{17}$$

The main studied objective in this project focuses on the capacity deferral to reduce the peak load at the feeder level. Then the optimization model becomes the following form:

$$\min\ \ \sum_{i=0}^{N-1} (E^{step}[\mathrm{i}] + D_{net}[\mathrm{i}])^2 \tag{18a}$$

$$s.t. E_{LB}^{step}[i] \le E^{step}[\mathrm{i}] \le E_{UB}^{step}[i] \tag{18b}$$

$$E^{step}[\mathrm{i}] + D_{net}[\mathrm{i}] \le Feeder_{EnrgyLmt}^{step} \tag{18c}$$

$$i = 0, \dots, N-1 \tag{18d}$$

In general, this is a quadratic optimization problem. It has the unique optimal solution and has the highly efficient algorithm to solve this problem. The solver used in this project is CVXOPT, which is a Python-based open source convex optimization toolbox.

3.3.1.3 Building Energy Allocation

By solving the above optimization model for every 10-minute interval, a solution array will be obtained, which includes $N = 36$ values for the proposed energy allocation of every 10-minute interval in the following 6 hours. The control process will update this array each 10 minutes; therefore, only the first element $E^{step}[0]$ in the solution array will be used for energy allocation for each specific building.

The following algorithm is designed for the energy allocation process:

Input: Aggregated energy allocation $E^{step}[0]$ for all involved buildings

Output: Energy allocation for each building $E_b^{step}[0]$, $b = 1, \dots, B$

Step 1: Determine the baseline of energy allocation for each building, which is the minimum forecasted energy value $E_{min}^b[0]$ at next time step.

Step 2: Calculate the energy allocation priority for each building.

$$\Delta_b = E_{max}^b[0] - E_{min}^b[0] \tag{19}$$

$$w_b = \Delta_b \Big/ \sum_{b=1}^{B} \Delta_b \tag{20}$$

where

w_b = The priority of building with index b.

For Step 2, he energy allocation priority determines how much energy will be allocated to the corresponding building besides the given minimum forecasted energy value. In general, high priority will get more energy from the energy budget $E^{step}[0] - \sum_{b=1}^{B} E_{min}^b[0]$.

Step 3: Energy to be allocated for building with index b in the next time step $E_b^{step}[0]$ is calculated using the following equation:

$$E_b^{step}[0] = E_{min}^b[0] + w_b * (E^{step}[0] - \sum_{b=1}^{B} E_{min}^b[0]) \tag{21}$$

3.3.2 Implementation Structure

The building aggregator is implemented using Python programming language on a Windows desktop at INL. Figure 25 shows the implemented modules in the aggregator. In general, a MQTT client is deployed on the Node-Red platform to receive the forecasted building energy limits and to send the building energy set points. A data preprocessing module will process the received energy limits data to ensure that they are ready for the optimization modeling. The optimization model construction module creates the necessary matrices to build the standard form for the defined optimization problem. Then, this model is to be solved using the CVXOPT solver. The obtained solution is the aggregated building energy amount. The building energy allocation module assigns the specific energy allocation for each building according to the designed algorithm. There is a data logging module in the building aggregator to save the historical data for result analysis. The stored data includes all received forecasted building energy limits at each time step and all the calculated building energy set points at each time step.

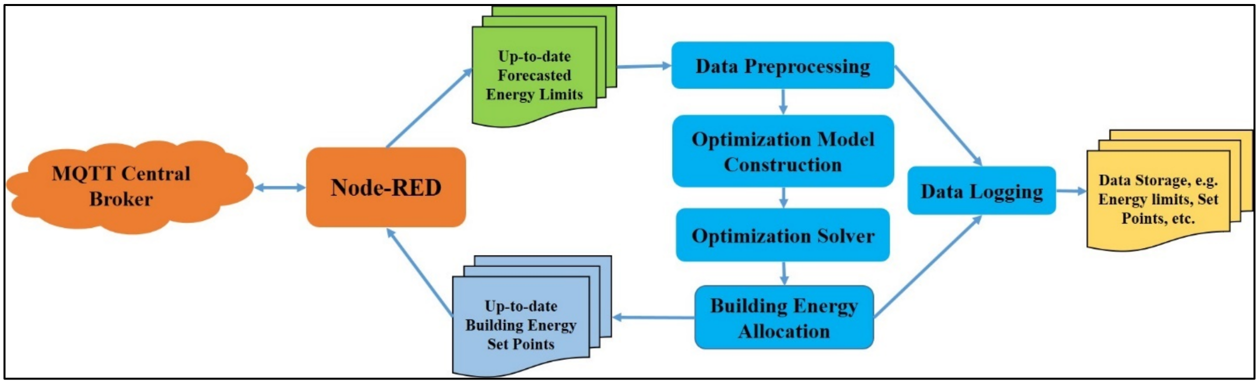

Figure 25. Building aggregator implementation modules and framework at INL.

3.4 Building Level Control

3.4.1 ANL Building Level Control

3.4.1.1 ANL System Architecture

The EV-Smart Grid Interoperability Center at ANL is pursuing an open-source approach to monitor and control networked devices to minimize barriers to commercial implementation of smart energy management. The IoT revolution could have both great business and technological impacts. These impacts have caused an influx of research and development in the IoT domain. The IoT does not have a one-size-fits-all solution. IoT solutions often require pulling together different device Application Programming Interfaces (APIs), abstracting, encapsulating and aggregating data, as well as routing the data to the appropriate places in the IoT pipeline with the expectation of providing value (control, analytics, etc.). When performing research and development in this space, developers need an IoT platform that is capable of rapid development and deployment that makes it easier for developers at all levels to create exciting new applications. Fortunately, IoT software developers are providing very scalable, extensible applications as open-source allowing other developers to utilize and further develop their applications freely. The ANL EV-Smart Grid Interoperability Center decided to leverage these open-source tools to create an IoT Common Integration Platform called CIP.io (pronounced as “sip-e-o”).

In any application enablement platform a gateway is needed as an interface between devices and other components of the platform. The gateway communication protocol is very important because it must be lightweight, extensible, scalable, and standardized. CIP.io utilizes the OASIS MQTT protocol standard. MQTT is a machine-to-machine/IoT connectivity protocol. It was designed as an extremely lightweight publish/subscribe messaging transport that can reliably scale to provide secure communications for billions of devices and trillions of messages. Within the MQTT protocol, a message broker acts as the gateway decoupling the many MQTT clients that subscribe and publish to topics on the broker. MQTT has strong open-source support. CIP.io leverages Mosquitto, an open-source MQTT broker, that is easy to install and configure for secure communication.

CIP.io is a combination of open-source tools each with a very specific task and purpose. Figure 26 shows the system architecture of CIP.io. CIP.io utilizes a global MQTT broker on the wide area network (WAN) bridged to local MQTT brokers on a local area network (LAN). The ability to bridge MQTT brokers allows system administrators to decide what information to keep on the local MQTT broker and what information to share to the global WAN MQTT broker. The global WAN MQTT broker is the gateway to individual building CIP.io platforms and the outside world. This allows other MQTT clients (HIL applications, smart-phone apps, etc.) to interact with the CIP.io platform from the Internet via the standardized MQTT protocol. Other services subscribing to the global WAN MQTT broker include a historian database and visualization applications.

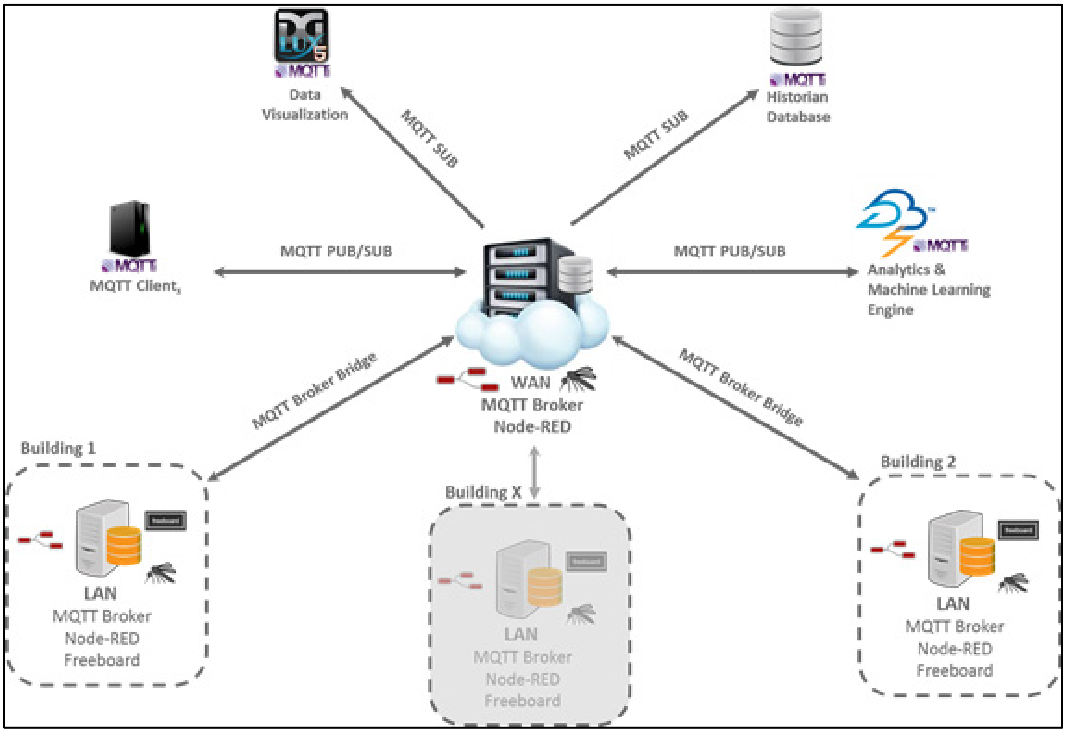

Figure 26. CIP.io system architecture.

A system controller is needed to provide local or global monitoring and control of devices and applications. At a local level, a system controller will interface with devices, reading sensors and controlling actuators, converting device protocols to MQTT and vice-versa, and interfacing with visualization applications and storage databases as shown in Figure 27. At a global level, a system controller will interface with other web-based systems to aggregate data from diverse web services. CIP.io utilizes IBM's open-source Node-RED as a system controller. Node-RED is described as the "visual tool for wiring the Internet of Things." Within the Node-RED environment, nodes are wired together to create flows, these flows perform a specific task. Node-RED allows browser-based flow editing with real-time debugging and deployment options enabling rapid application development. Node Red is built on Node.js, taking full advantage of its event-driven, non-blocking model. Node.js' package repository, npm, is the largest ecosystem of open-source libraries in the world. CIP.io utilizes the Node-Red Freeboard node for data visualization as well as the built-in Node-Red dashboard nodes.

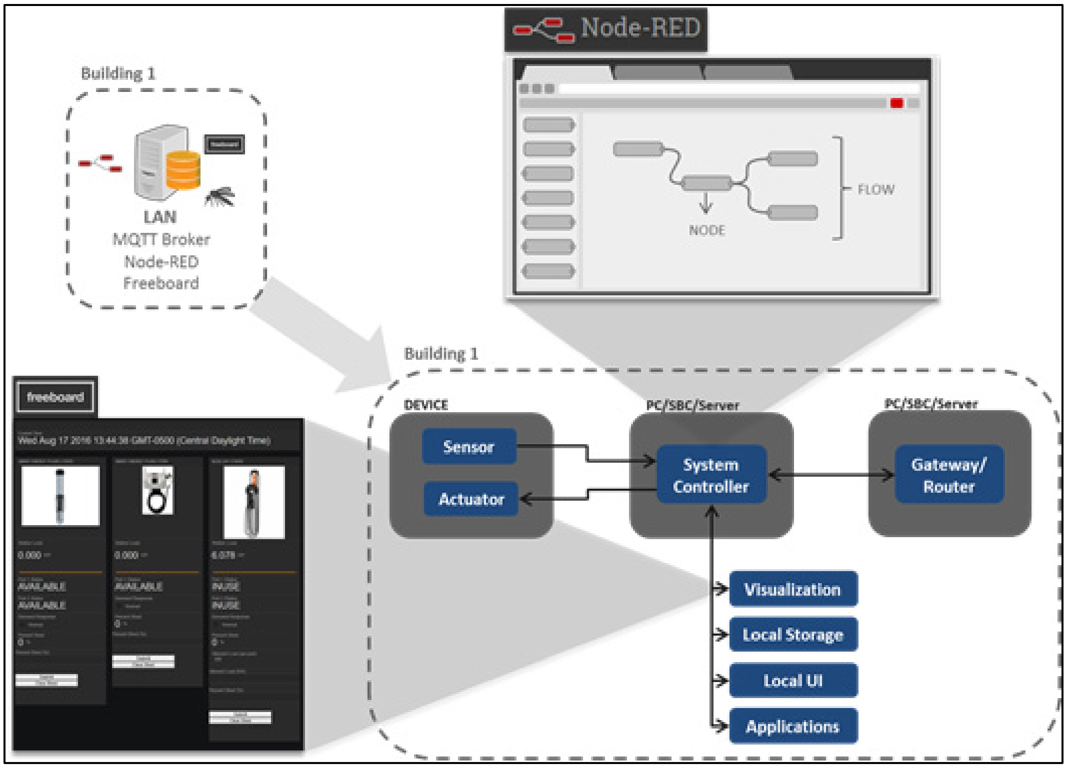

Figure 27. Breakout of CIP.io building level architecture.

Within the design of any IoT platform, security considerations are paramount. Every component and interface in CIP.io is a potential attack vector; therefore, well-established and widely accepted security mechanisms such as encryption (SSL/TLS), authentication, and authorization have been deployed. For example, each Node-RED web user interface (UI) utilizes HTTPS for secure communication and authentication. For authentication and authorization, Node-RED users are provided with usernames and passwords with the potential for read/write access configuration. Each MQTT broker in CIP.io utilizes an SSL/TLS connection with authentication and authorization for each device/user. Access control lists are utilized to define what topics each user can publish and subscribe to. Security is always being considered and reexamined with continuing efforts focusing on data security, privacy, data integrity, and network security.

3.4.1.2 Building Control Strategy

The ANL-implemented smart charging control algorithm implements the following priorities:

1. The demand charge limit for the building is top priority. The V1G smart charging algorithm's goal is to never exceed this limit. However, the algorithm currently does not shut down individual PEVs. Therefore, the only case in which the demand charge limit for the building will be exceeded is when reducing all PEV charging to their minimum rate results in the building load to exceed the demand charge limit.
2. PEV charging priority is based on instantaneous missing capacity (AC kWh) for each vehicle. The algorithm will attempt to meet all PEV energy needs by their departure time within the demand charge limit constraints.

The control of the ANL algorithm is based upon instantaneous missing capacity (AC kWh).

$$DeltaCapacity\ (kWh) = TargetCapacity\ (kWh) - Actual\ Capacity\ (kWh) \tag{22}$$

$$PredictedAddedCapacity\ (kWh) = AC\ Power\ (kW) * DepartureTimeLeft\ (h) \tag{23}$$

$$Inst.MissingCapacity\ (kWh) = DeltaCapacity\ (kWh) - PredictedAddedCapacity(kWh) \tag{24}$$

A positive instantaneous missing capacity means that at the instantaneous charge rate (AC kW), the PEV will not meet its goal by departure time. Conversely, a negative instantaneous missing capacity means that at the instantaneous charge rate (AC kW), the PEV will meet its goal by the departure time. Other control strategies can be implemented as long as the same data structures are utilized within the flow.

The algorithm controls each PEV's charge rate to optimize its charge schedule to ensure the PEV's energy need is met by its departure time, but ultimately defaulting to maintaining the site's power consumption below the site's limit (AC kW). For every time step, the available PEV charging power is calculated and the necessary control is applied to maintain the Smart Energy Plaza's active power underneath the site's limit.

If there is a surplus of available PEV charging power, each PEV/EVSE (Electric Vehicle Supply Equipment) pair is ranked (maximum to minimum) based on its instantaneous missing capacity (AC kWh). The control algorithm then determines how to appropriately increase each PEV in order to distribute the available PEV charging power. The current version of the algorithm determines how much each PEV can be increased before meeting its individual maximum power limit (minimum of PEV On-Board Charger Module (OBCM) rating and EVSE ampacity/power). The algorithm then starts with the PEV with the highest instantaneous missing capacity and will increase this PEV to its maximum power limit if it does not exceed the available PEV charging power and if this PEV's amperage utility is greater than 90%. The PEV's amperage utility metric provides the algorithm a sense of how well each PEV is using the available ampacity. Amperage utility is a ratio of instantaneous current draw of the PEV to the AC EVSE ampacity (duty cycle converted to amps).

$$Amperage\ Utility = \frac{PEV\ AC\ Current\ (Arms)}{EVSE\ Ampacity\ (Arms)} \tag{25}$$

The amperage utility check will not allow a PEV's power to be increased if it is currently not utilizing its current available power, such as when the PEV is topping off towards the end of a charge session. Hence, a PEV may have a higher instantaneous missing capacity than another PEV but it will not be increased if its amperage utility is not greater than 90%. The algorithm continues increasing each ranked PEV to its maximum power until the available power is distributed among the charging PEVs.

If there is a deficit of available PEV charging power, each PEV/EVSE pair is ranked (minimum to maximum) based on its instantaneous missing capacity (AC kWh). The control algorithm then determines how to appropriately decrease each PEV in order to curtail PEV charging power below the available PEV charging power signal. The algorithm then starts with the PEV with the lowest instantaneous missing capacity and will decrease this PEV to its minimum power limit. The algorithm continues decreasing each ranked PEV to its minimum power until the PEV charging power is below the available PEV charging power signal.

3.4.2 NREL Building Level Control

3.4.2.1 NREL System Architecture

Figure 28 shows the architecture of NREL's system for the GM0085 Project. Building load is generated by a load bank with a pre-programmed load profile and a real-time grid simulator emulates grid behavior. The NREL aggregator receives real-time total building load data (controllable and uncontrollable building loads) from RTDS. It calculates a building energy profile (*Emin* and *Emax*) based on a building load forecast and EVSE energy requests from the EVSE user input system, and then publishes it to the ANL MQTT broker. Upon receiving a set point value from the INL aggregator, the NREL aggregator allocates energy set point values for each controllable load based on their priority and controls loads by sending commands to each device through MQTT message publishing.

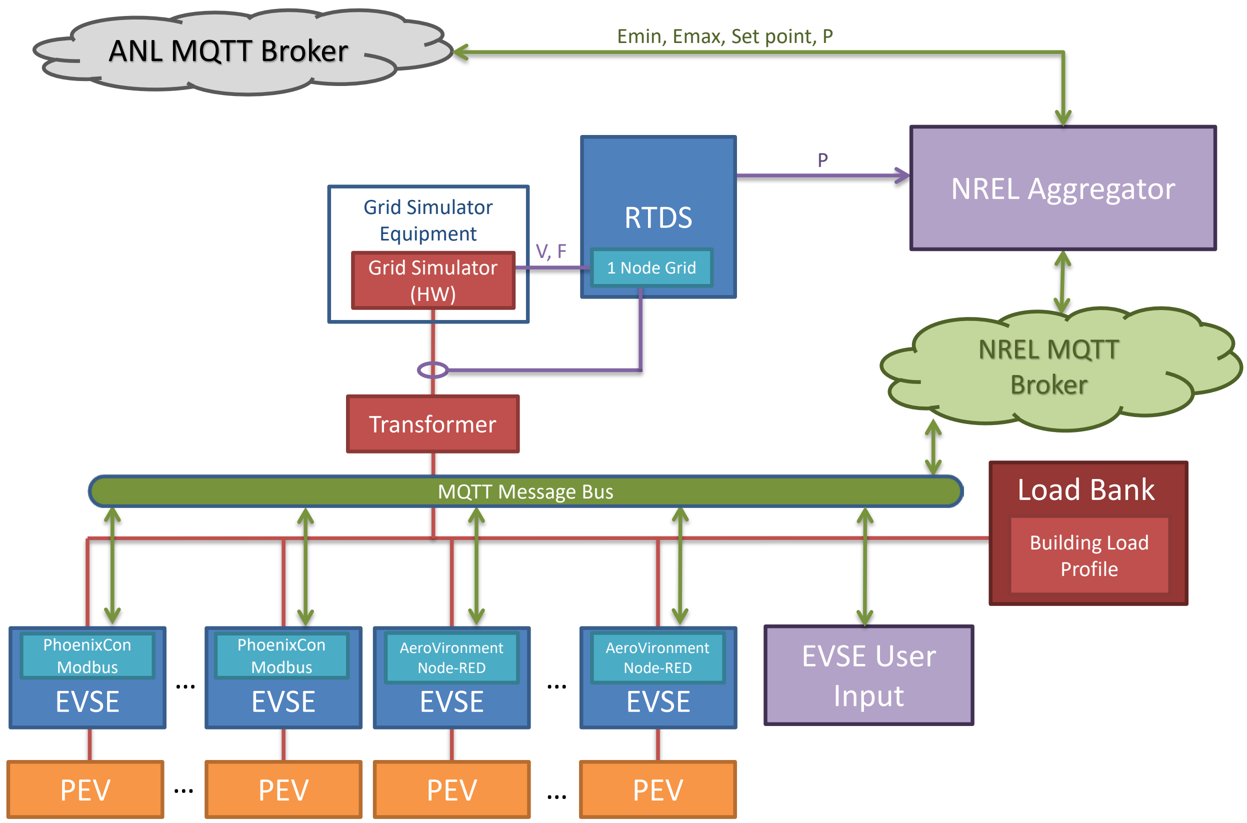

Figure 28. Architecture of NREL system for GM0085.

The NREL aggregator uses the load bank building load profile as a building load forecast. However, the EVSE load is not included in the profile and the actual building load measured by RTDS is different from the forecasted value. The NREL aggregator adjusts the forecast value every 10 minutes based on the error between the forecast and the actual load and uses the adjusted forecast value in the calculation of *Emin* and *Emax*.

3.4.2.2 Building Control Strategy

The local building controller adjusts the EVSE load when the total building load reaches a threshold value. The adjusted amount of EVSE load is dependent on the requested energy amount and the departure time. The controller calculates how much charging power of each station can be reduced when campus load reaches a threshold value. The algorithm should guarantee that each station delivers the requested energy amount by the departure time with this adjusted charging power. The algorithm calculates a new power value for charging as follows:

1. Find a list of charging stations k that can provide the requested energy amount by the departure time.
2. For each k, calculate a new charging value.

$$P_k^{new} = \frac{Energy_k^{requested} - Energy_k^{delivered}}{T_k^{departure} - T_{present}} \tag{26}$$

3. Calculate the total power that is reduced by charging management.

$$P_{reduced} = \sum_k \left(P_k^{old} - P_k^{new}\right) \tag{27}$$

Notice that if more stations are on the list, more power reduction is possible by charge management. If there is no charging station on the list, there is no power reduction possible by charge management.

3.4.2.3 Energy Limit Forecast for the Aggregator

Uncontrollable building load is generated by a load bank with a pre-programmed load profile. The load profile is from a real commercial building load. Load by EVSE is the only controllable building load. The NREL aggregator receives the total building load (uncontrollable and controllable loads) from RTDS and gets EVSE energy requests from the EVSE user input system. With the total building load and the EVSE energy requests, it calculates *Emin*/*Emax* for the INL aggregator. *Emin*/*Emax* data consist of 11 values. The first six values represent 10-minute interval forecast energies followed by 1-hour interval forecast energies. If no cars are connected to charges, the values of *Emin* and *Emax* are the same because there is no controllable load.

3.4.3 PNNL Building Level Control

The PNNL building and PEV charging interface to the GM0085 system consists of five elements (see Figure 29). The two elements in the purple boxes enable PNNL to publish building load and PEV charging data and subscribe to set point data on the ANL-hosted MQTT broker. The two elements in the blue boxes are connections to the GM0062 Project vehicle to building integration system to publish and subscribe to data on PNNL's VOLTTRON system, including PEV charging, PV generation, and building data. The remainder of the processes in Figure 29 are functions that enable selecting, formatting, and parsing data.

The ANL-hosted MQTT broker connection (purple box in Figure 29on the bottom left) enabled PNNL to subscribe to the INL-published, set point topic. These messages began with DOE/GM0085/PNNL/Setpoint and were converted from json to objects using the json module before being passed to the "Broker Message Processor" function block. These messages were processed by the Broker Message Processor block using its four functions: (1) calculate message latency and echo received messages back to transmitter; (2) store MQTT messages in the file Forecast_Messages.txt; (3) display communications latency data (~100 milliseconds ANL ⇔ PNNL); and (4) read the INL commanded set point data. The commanded set point data was used by the GM0062 Project system to prioritize power delivery to the vehicles based on their energy requirements, maximum charging rate, and remaining time to charge.

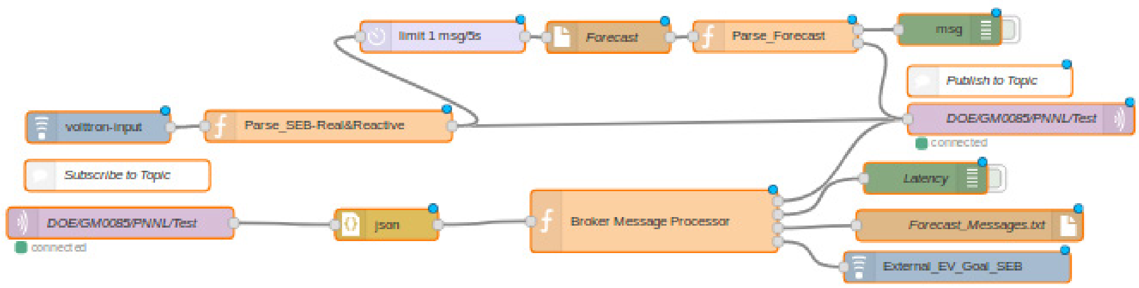

Figure 29. PNNL Node-RED interface to the GM0085 control and communications system.

The PNNL VOLTTRON input node (top left) enables the PNNL GM0085 Node-RED system to subscribe to VOLTTRON data from the PNNL GM0062 Project vehicle to building integration system. Node-RED functions are then used to process the PNNL VOLTTRON data. The Parse_SEB-Real&Reactive function parses PNNL building real and reactive power data sending one copy directly to the MQTT broker and saving the second copy to a file. The saved data is used by a Python routine to develop the forecast as described below. The system also processes and stores vehicle charging power, building power, and PV power data in text files for post-processing analyses.

The approach used to forecast energy requirements over the 10-minute, 20-minute, 30-minute, 40-minute, 50-minute, and 60-minute intervals and 2-hour, 3-hour, 4-hour, 5-hour, and 6-hour intervals used a short Python routine designed to maximize energy delivered to charging PEVs during their remaining time connected. This forecast routine read stored GM0062 Project data (e.g., remaining energy needed, charge time remaining, and maximum charging rate) for each PEV charging to calculate the minimum charging energy (*Emin*) needed over each forecast time interval to deliver the PEV fully charged. The maximum charging energy was the sum of the maximum charging rate for all connected vehicles.

The system communication performance was formally tested on December/19, 2018.

3.5 Commercial Control Strategy Performance

In the control framework for multiple commercial buildings where PEVs are charging that are connected to a distribution feeder, there are two main control entities, the buildings and the feeder, whose benefits try to be maximized. Usually, the buildings and the feeder can have their own objectives/interests, which are competing with each other. What is best for buildings (e.g., reducing building peak load), may not be best for the feeder (e.g., reducing feeder peak load). It is not always possible to provide the maximum benefit to the buildings and the feeder at the same time. Therefore, the designed control strategies that coordinate building loads need to manage the trade-offs between control requirements as follows:

- Only consider needs of the buildings
- Balance needs of the buildings and the feeder
- Only consider needs of the feeder.

The impact on the distribution feeder of PEV charging controlled by commercial buildings, with and without aggregator support, has been studied using the developed testing platform. To quantify the value of controlling PEV charging, the following scenarios were studied:

- PEV charging controlled by the buildings without the aggregator
- PEV charging controlled by the buildings, coordinated by the aggregator
- Uncontrolled PEV charging.

The corresponding results and comparisons related to these scenarios are defined and analyzed in Sections 3.5.1, 3.5.2, and 3.5.3.

3.5.1 GM0062 Project Control Provides Maximum Benefit at Building Level

The designed building control strategies in GM0062 Project are to manage peak load at the building level. These building control strategies have been studied using the developed testing platform in this project. Figure 30 shows the results. The testing time is from 6:00 a.m. to 6:00 p.m. Results include scaled building power for the three buildings at ANL, NREL, and PNNL under both uncontrolled and building controlled scenarios. The building loads were scaled by using different multipliers (i.e., ANL multiplier = 35, NREL multiplier = 35, PNNL multiplier = 7). These multipliers are used to simulate the load on a feeder system and make them have the enough impact on the feeder system for the control benefits investigation. Results show that GM0062 Project building control shows benefit at the building level by managing peak load to minimize demand charges. Building peak load is reduced when PEV charging is controlled by BEMSs.

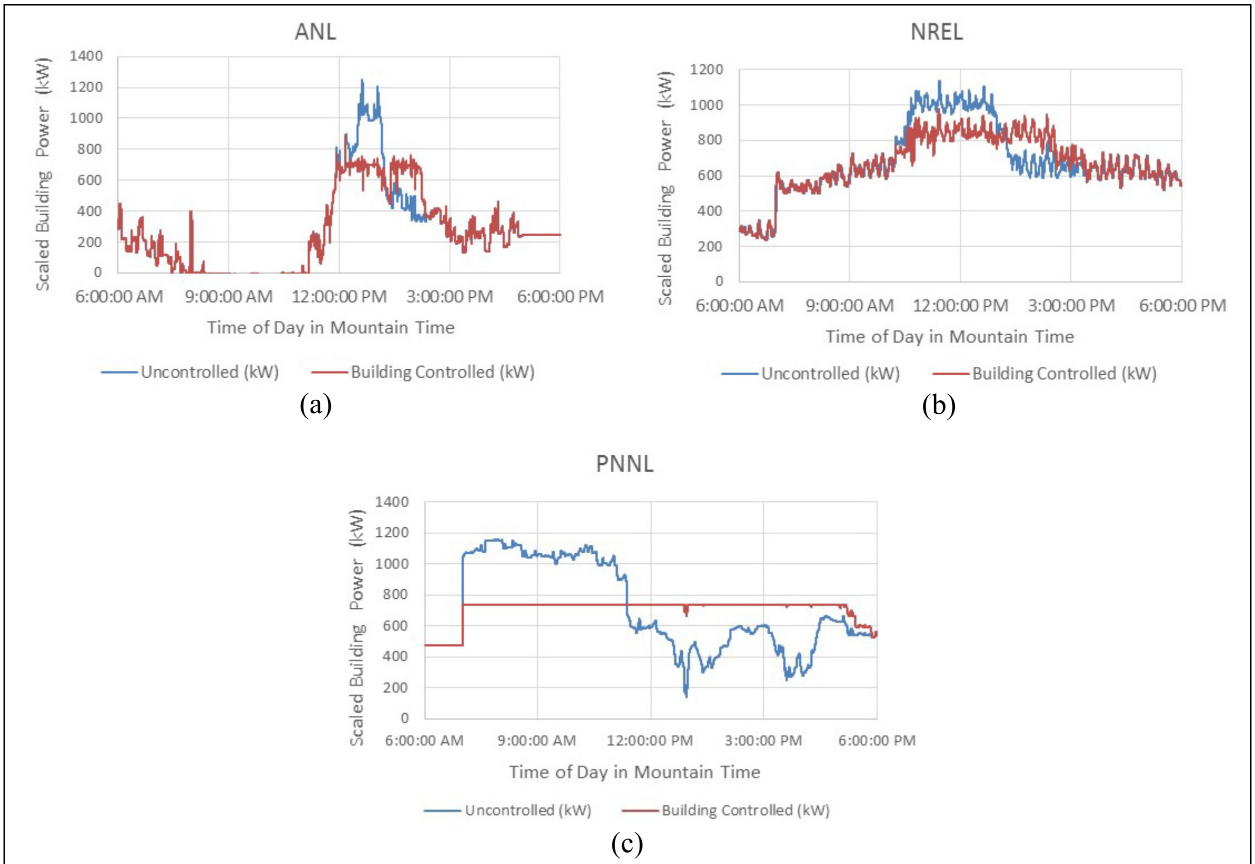

Figure 30. Scaled building power profile for the three buildings at (a) ANL, (b) NREL, and (c) PNNL under the uncontrolled and building controlled scenarios.

3.5.2 GM0062 Project Control Provides Less Benefit at Feeder Level

Based on the scaled power profiles for the three buildings at ANL, NREL, and PNNL, the aggregated power profiles for the buildings are shown in Figure 31 for both uncontrolled and building controlled scenarios. The aggregated power profile at the feeder level shows that the peak load at the feeder level under the building control is not reduced comparing with the scenario when PEV charging is uncontrolled. This is because GM0062 Project control maximizes benefit at the building level. Peak feeder loads are about the same in uncontrolled and building controlled scenarios because building peaks are not coincident (see Figure 31(a) and Figure 31(b)).

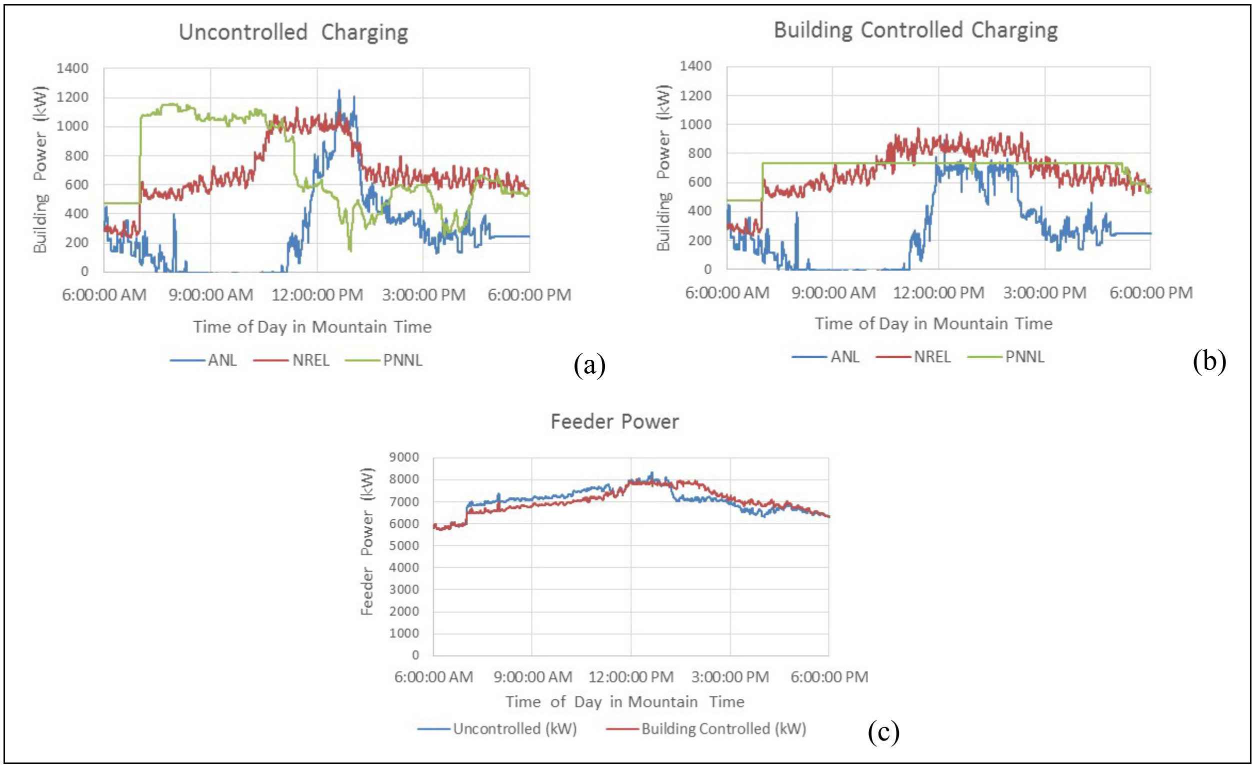

Figure 31. Power load profiles for the three buildings at ANL, NREL, and PNNL. (a) power load profile under the uncontrolled scenario; (b) power load profile under the building controlled scenario; (c) aggregated power load of at the feeder level under the uncontrolled and building controlled scenarios.

3.5.3 Aggregator-assisted Control Performance

Multiple tests performed in this project demonstrate that the platform developed for aggregator-assisted control is functional and operated successfully. Two scenarios were tested in this project. In both scenarios, the platform was able to share real-time data securely and reliably between INL, ANL, NREL, and PNNL.

Figure 32 shows the results of the feeder power profiles of uncontrolled, building controlled and aggregator-assisted controlled scenarios for two different days. Results show that, unfortunately, peak feeder load is about the same in the uncontrolled and aggregator-assisted scenarios.

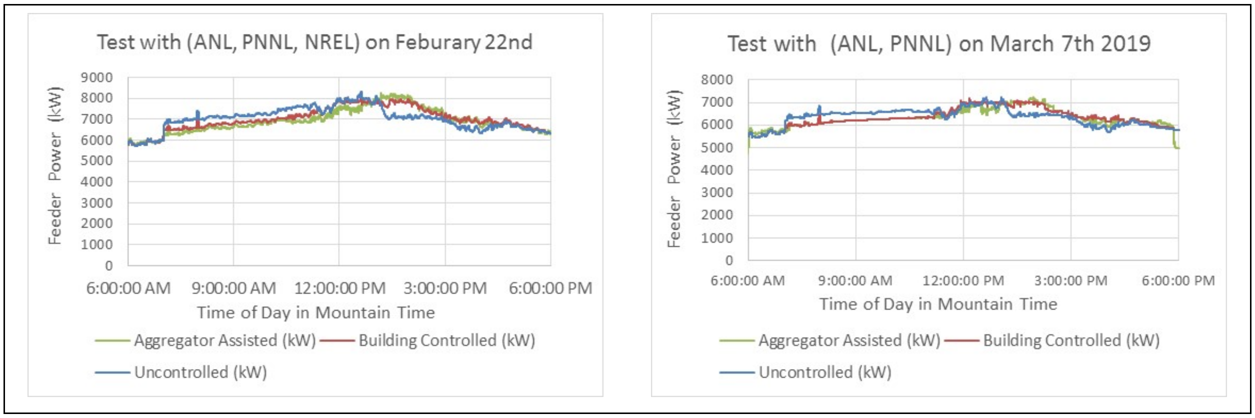

Figure 32. Comparisons between uncontrolled, building controlled, and aggregator-assisted controlled scenarios in two different days.

Figure 33 shows the results of voltage deviations at the feeder level for the three buildings and the three different scenarios. Voltage deviations are about the same in the uncontrolled, building controlled, and aggregator-assisted controlled scenarios for the three buildings. This is because the building control and aggregator-assisted control were designed to provide peak load reduction not voltage regulation. However, the obtained results show that the developed testing platform is capable to perform the grid impact studies from a different perspective. This means the developed platform is useful for future grid impact studies when other objectives are going to be investigated.

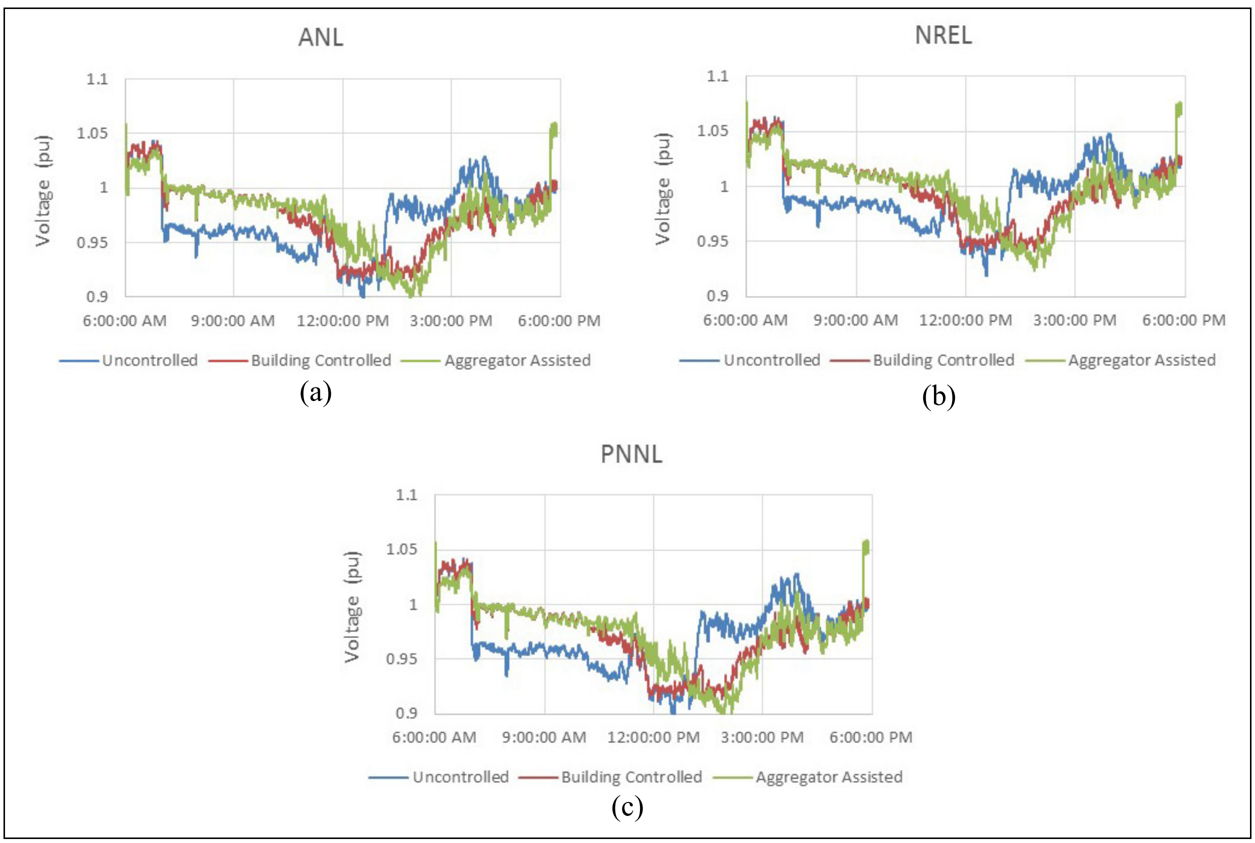

Figure 33. Voltage deviations for the three buildings at (a) ANL, (b) NREL, and (c) PNNL at the feeder system under uncontrolled, building controlled, and aggregator-assisted controlled scenarios.

3.6 System Design Analysis and Future Work

3.6.1 Aggregator-assisted Control System Diagram

Figure 34 shows the system diagram of the aggregator-assisted control framework. The aggregator receives the energy limits forecast from the buildings. The energy limits forecast is maximum and minimum building energy forecast for the next 6 hours in current designed system. These limits forecast is based on the PEV state forecast and PEV charging assumptions shown in Figure 34. Each building has its own energy limits forecast for the next 6 hours based on specific PEV charging assumptions in the three buildings at ANL, NREL, and PNNL. Detailed format of energy limits forecast is discussed in Section 3.3.

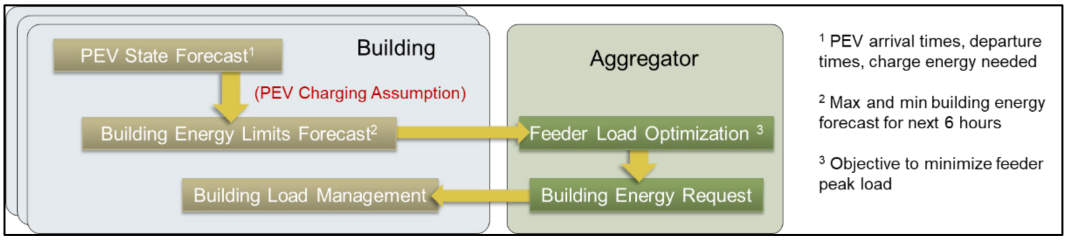

Figure 34. Aggregator-assisted control framework.

The aggregator creates the building energy requests by performing the feeder load optimization according to a specific objective (e.g., feeder peak load). The generated building energy requests are sent to building load management systems. In the current system design, the aggregator always returned each building to its minimum limit for the next time step, as shown in Figure 35 for the energy request of ANL's building. Due to the target of capacity deferral, the objective function of reducing peak load was modeled as a quadratic function. Minimizing the quadratic objective function forces the building energy request to be as small as possible within the feasible energy boundaries.

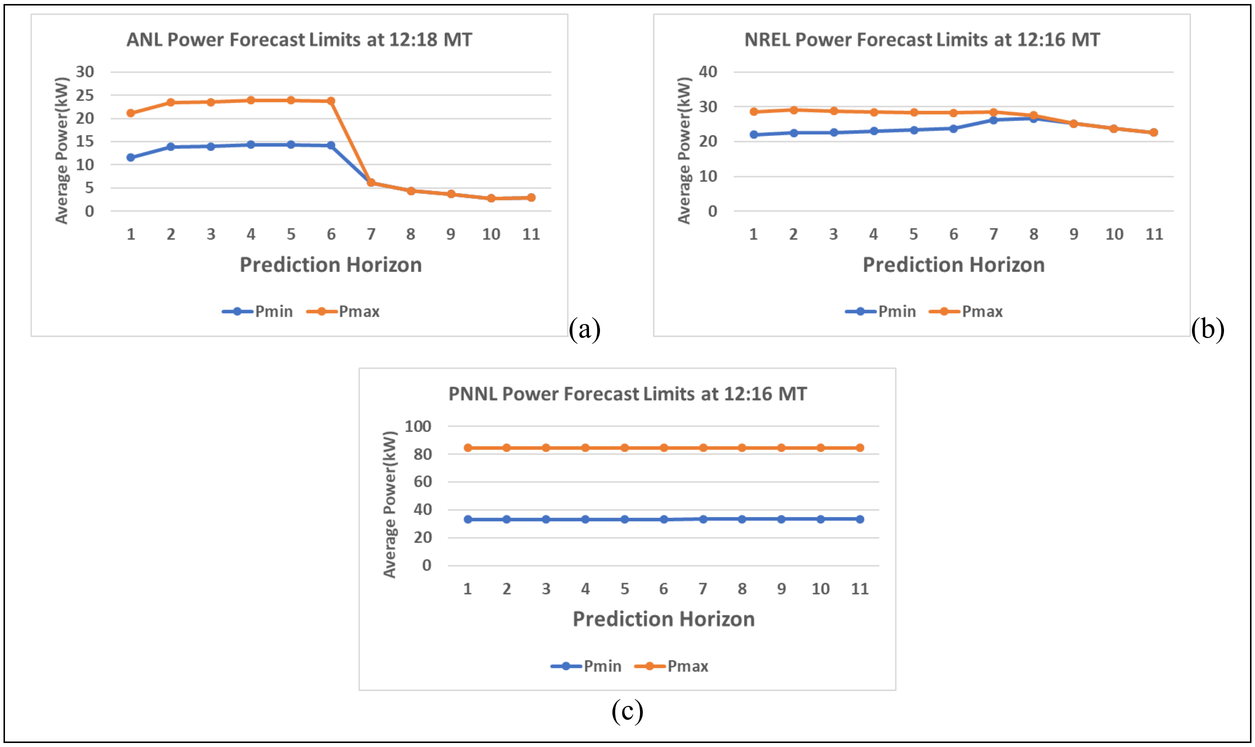

Figure 35. Energy limits forecast for (a) ANL, (b) NREL, and (c) PNNL, with a prediction horizon of time range 12:10-12:20 Mountain Time.

As discussed in previous result analysis, aggregator-assisted control cannot provide benefits on peak reduction based on the current system design structure. The building energy limits forecast algorithm and buildings aggregator algorithm were developed independently at the component level. The building energy limits forecast was defined first and everything was built around it. The proper functionality of optimization in the aggregator is determined by meaningful limits/bounds. When buildings create the energy limit forecast, implicitly required assumptions about PEV charging to be made at the building level. The building forecast depends on an assumption of how the vehicles will be charged during the prediction horizon. This forced a solution at the building level, defeating the purpose of the aggregator. The aggregator needs the bounds of charging flexibility not bounds based on an arbitrary charging assumption. Therefore, algorithms should be designed at the system level not the component level. Figure 36 shows a demonstration of energy limits (*Emin* and *Emax*) and energy set points for ANL.

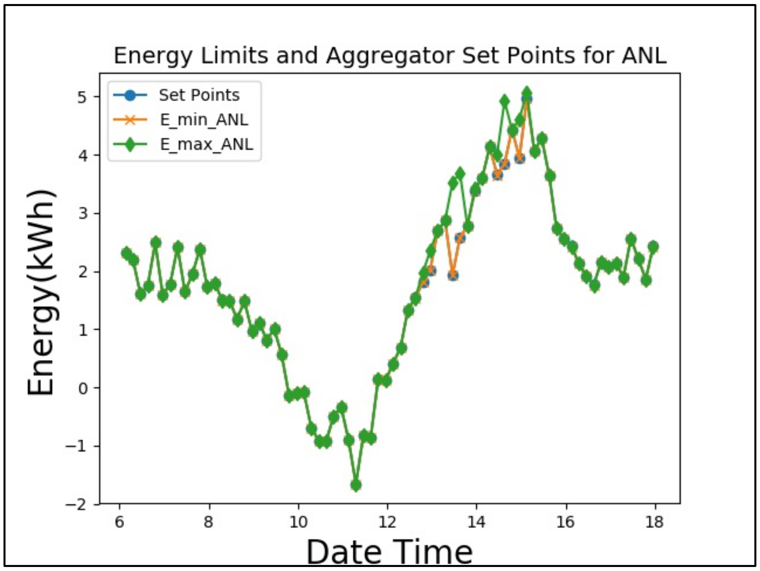

Figure 36. Demonstration of energy limits (*Emin* and *Emax*) and energy set points for ANL from 6:00 to 18:00 (6:00 a.m. to 6:00 p.m.).

3.6.2 Future Work

Due to the competing interests between the buildings and feeder, a trade-off must be made when conducting the aggregator-assisted control to coordinate the PEV charging in multiple buildings. Figure 37 shows a potential control framework that can be used to improve performance of aggregator-assisted control in future research work. As shown in Figure 37, the framework includes steps to:

1. Prioritize and value building needs and feeder needs
2. Divide charging flexibility between building needs and feeder needs according to priorities
3. Send to the aggregator the bounds of charging flexibility allocated to meet feeder needs
4. Maximize feeder benefits within the bounds of charging flexibility
5. Send optimal energy request to the buildings.

Among these steps, key operations are to prioritize and value the needs between buildings and the feeder, then divide the corresponding charging flexibility. The bonds of charging flexibility will be meaningful information for the aggregator to optimize its decisions, which will try to provide the most benefits at the feeder level by using the allowed charging flexibility from the building level.

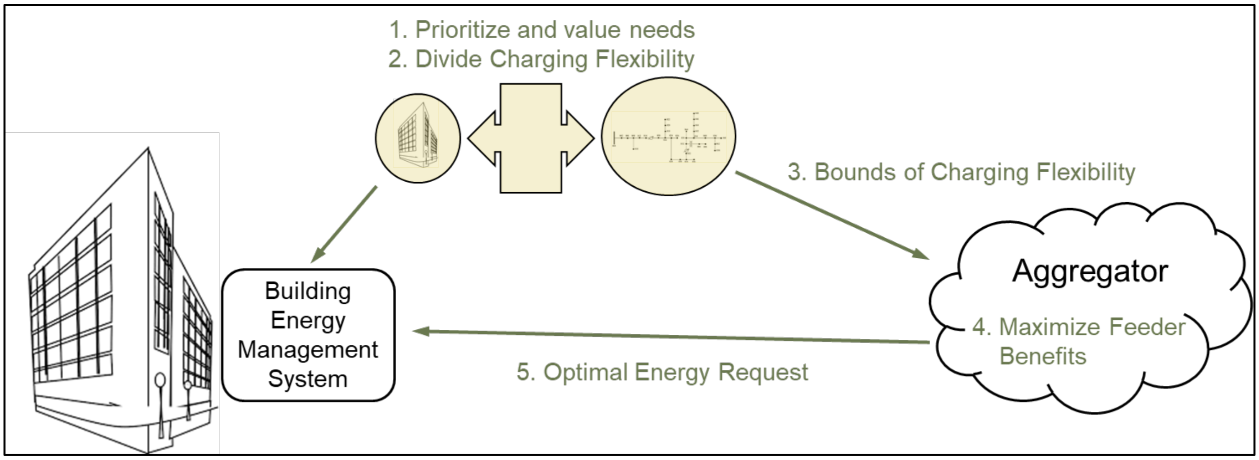

Figure 37. Potential control framework to improve performance of aggregator-assisted control.

4. REFERENCES

1. Smart, J., "Plugged In: How Americans Charge Their Electric Vehicles," https://avt.inl.gov/sites/default/files/pdf/arra/PluggedInSummaryReport.pdf, Web page visited January 12, 2019.

2. Scoffield, D., J. Smart, S. Salisbury, and M. Kirkpatrick, *Investigating the Usefulness of Grid-Connected Plug-in Electric Vehicles as Controllable Loads*, INL/EXT-14-33966, Idaho National Laboratory, December 2014, https://avt.inl.gov/sites/default/files/pdf/phev/InvestigatingTheUsefullnessOfGridConnectedPHEVasControllableLoads.pdf, Web page visited January 12, 2019.

3. Schey, S., D. Scoffield, and J. Smart. "A First Look at the Impact of Electric Vehicle Charging on the Electric Grid in The EV Project," *World Electric Vehicle Journal*, Vol. 5, No. 3, September 2012, pp. 667-678, DOI: 10.3390/wevj5030667.

4. Yi, Z. and D. Scoffield, "A Data-Driven Framework for Residential Electric Vehicle Charging Load Profile Generation," 2018 IEEE Transportation Electrification Conference and Expo (ITEC), Long Beach, CA, 2018, pp. 519-524, DOI: 10.1109/ITEC.2018.8450228.

5. Pacific Gas & Electric, "Understanding Energy Use and Prices," https://www.pge.com/nots/rates/tariffs/energy_use_prices.shtml, Web page visited January 12, 2019.

6. Pacific Gas & Electric, Photovoltaic and renewable auction mechanism map, https://www.pge.com/en_US/for-our-business-partners/distribution-resource-planning/distribution-resource-planning-data-portal.page, Web page visited.

7. California Energy Commission – Tracking Progress, https://www.energy.ca.gov/renewables/tracking_progress/documents/statewide_energy_demand.pdf, downloaded on January 11, 2019.

Appendix A

Projection of Electric Vehicle Stocks in California

A-1. METHODOLOGY AND RESULTS

To develop our forecast of EV penetration in California, we began with historical data on California EV sales (sum of battery, plug-in hybrid and fuel cell EVs) from January 2011 through August 2018 from Auto Alliance [A-1], with additional data from Veloz [A-2]. These data were fit to an exponential function with the following functional form:

*Annual sale*s = exp(*A* * *Year* + *B*)

The optimal fits of the coefficients for this equation are shown in Table A1.

Coefficient	Value	Standard Deviation
A	0.3875	0.0547
B	-769.9	110.2

Table A1. Optimal fit coefficients for California EV sales data. Sources: [A-1] and [A-2]

Extending this fit through 2030 results in an unrealistically large number of vehicle sales that far exceeds total annual vehicle sales (2.0 million in 2016, as derived from [A-1]). To address this issue, a sigmoidal function was developed to "bend over" the exponential curve in outlying years to reach a total EV stock of 6.7 M vehicles in 2030, which is consistent with the high end of statewide EV penetration estimates from Southern California Edison [A-3]. (By comparison, the state's own goal is 5 M vehicles [A-4].) This sigmoidal function multiplies the projected exponential fit of future vehicle sales by a reduction factor that tapers from 76.4% in 2019 to 4.2% in 2030, using the following functional form:

Reduction factor = 1 – 1/[1 + 1/exp(*C* • *Year* + *D*)]

The coefficients for this equation are shown in Table A2, which were obtained by forcing the sigmoidal function to have a value of 50% in 2022 and 10% in 2027.6.

Coefficient	Value
C	0.3924
D	-793.4

Table A2. Coefficients of EV sales sigmoidal function.

In order to calculate EV stock from EV sales, a vehicle survival function was used from Bento et al. [A-5] with the following function of model year *m* and age *a* :

Vehicles (*m* , *a*) = *Vehicles* (*m* , *a* – 1) • {1 – 1/[*E* + *F* • exp(*G* • *a*)]}

Where *Vehicles* (*m* , 0) are the number of vehicles sold initially. The coefficients for this equation are shown in Table A3.

Coefficient	Value
E	2.724
F	314.03
G	-0.275

Table A3. Coefficients of passenger car survival function. Source: [A-5]

The stock model was initiated for model year 2011 and provided with historical EV sales data for 2011 through 2018 (Auto Alliance data through August 2018 were projected through the end of 2018). Because sales grow so rapidly, particularly in the early years, the effect of using a vehicle survival function is modest; if instead all vehicles sold are assumed to last indefinitely, the projected vehicle stock in 2030 would be only 8% larger.

To obtain the final result of vehicles per household, we used the California Energy Commission forecast of California households through 2030 [A-6] to divide vehicle stocks by number of households. The resulting EV penetrations obtained were 3.9% in 2018, 7.2% in 2020, 23.8% in 2025 and 45.3% in 2030.

A-2. REFERENCES

A-1. Auto Alliance, *Advanced Technology Vehicle Sales Dashboard*, U.S. Light-Duty Advanced Technology Vehicle (ATV) Sales (2011–2018)," https://autoalliance.org/energy-environment/advanced-technology-vehicle-sales-dashboard/, downloaded on January 10, 2019.

A-2. Veloz, monthly and cumulative sales of electric vehicles between December 2010 and November 2018, for California and the U.S., Published December 5, 2018, http://www.veloz.org/wp-content/uploads/2018/12/11_nov_2018_Dashboard_PEV_Sales_veloz.pdf, downloaded on January 10, 2019.

A-3. Southern California Edison, *The Clean Power and Electrification Pathway, Realizing California's Environmental Goals*, November 2017, https://newsroom.edison.com/internal_redirect/cms.ipressroom.com.s3.amazonaws.com/166/files/20187/g17-pathway-to-2030-white-paper.pdf, downloaded on February 20, 2019.

A-4. Office of Governor Edmund G. Brown Jr., *Governor Brown Delivers 2018 State of the State Address: "California is Setting the Pace for America,"* January 25, 2018, https://www.ca.gov/archive/gov39/2018/01/25/governor-brown-delivers-2018-state-of-the-state-address-california-is-setting-the-pace-for-america/index.html, downloaded on February 20, 2019.

A-5. Bento, A., K. Roth, Y. Zuo, 2016, "Vehicle Lifetime Trends and Scrappage Behavior in the U.S. Used Car Market," white paper, UC Irvine, January 18, 2016, https://faculty.sites.uci.edu/kevinroth/files/2011/03/Scrappage_18Jan2016.pdf, downloaded on February 20, 2019.

A-6. California Energy Commission, 2017, "Revised Baseline STATEWIDE Mid Demand Case TN-222323, Form 2.2 - STATEWIDE: California Energy Demand 2018-2030 Revised Baseline Forecast - Mid Demand Case, Planning Area Economic and Demographic Assumptions," published January 22, 2018, https://efiling.energy.ca.gov/GetDocument.aspx?tn=222323&DocumentContentId=28716, downloaded on January 11, 2019.